Traffic

Published by John Wiley & Sons Ltd
doi:10.1111/tra.12245

Rerouting of Plant Late Endocytic Trafficking Toward a Pathogen Interface

Tolga O. Bozkurt[1,2], Khaoula Belhaj[1], Yasin F. Dagdas[1], Angela Chaparro-Garcia[1], Chih-Hang Wu[1], Liliana M. Cano[1] and Sophien Kamoun[1,*]

[1]The Sainsbury Laboratory, Norwich Research Park, Norwich, UK
[2]Current address: Department of Life Sciences, Imperial College London, London, UK
*Corresponding author: Sophien Kamoun, sophien.kamoun@tsl.ac.uk

Abstract

A number of plant pathogenic and symbiotic microbes produce specialized cellular structures that invade host cells where they remain enveloped by host-derived membranes. The mechanisms underlying the biogenesis and functions of host–microbe interfaces are poorly understood. Here, we show that plant late endocytic trafficking is diverted toward the extrahaustorial membrane (EHM); a host–pathogen interface that develops in plant cells invaded by Irish potato famine pathogen *Phytophthora infestans*. A late endosome and tonoplast marker protein Rab7 GTPase RabG3c, but not a tonoplast-localized sucrose transporter, is recruited to the EHM, suggesting specific rerouting of vacuole-targeted late endosomes to a host–pathogen interface. We revealed the dynamic nature of this process by showing that, upon activation, a cell surface immune receptor traffics toward the haustorial interface. Our work provides insight into the biogenesis of the EHM and reveals dynamic processes that recruit membrane compartments and immune receptors to this host–pathogen interface.

Keywords AVRblb2, effector, extrahaustorial membrane, haustorium, late endosome, *Phytophthora infestans*, RabG3c

Received 17 June 2014, revised and accepted for publication 25 November 2014, uncorrected manuscript published online 28 November 2014

Plants interact with a multitude of parasitic and symbiotic organisms. Plant cells accommodate some of these organisms inside specialized compartments that are typically separated from the plant cytoplasm by host-derived membranes (1–4). This interface is critical for the regulation and development of parasitic or symbiotic host colonization, for instance by enabling efficient macromolecule exchange. However, the mechanisms underlining the biogenesis and functions of this intimate host–microbe interface are poorly understood. We know little about the reprogramming of cellular and biochemical events that take place inside plant cells that are colonized by microbes (5–7).

An example of accommodation structure is the haustorium, a hyphal extension formed by some species of filamentous plant pathogens (fungi and oomycetes). Haustoria penetrate the plant cell in order to deliver virulence proteins, known as effectors, and acquire nutrients from the host (8–10). A host-derived membrane, called the extrahaustorial membrane (EHM), separates the haustorium from the invaded plant cells and delimits the haustorial interface. The extracellular space between the EHM and the haustorium is known as the extrahaustorial matrix (EHMx) (10–13). Together, the EHM and the EHMx compartments (referred to as EHM compartments in this article) form a critical interface between the host and the pathogen that is essential for parasitic infection by several fungal and oomycete pathogens. In addition, the plant vacuolar membrane (tonoplast) is often in close proximity to the EHM because the central vacuole occupies a large space within plant epidermal leaf cells (13–15). Although the tonoplast remains separated from the EHM by a thin layer of cytoplasm, it can be difficult to discriminate between these compartments during live cell imaging. Therefore, previous studies have not managed to discriminate between perihaustorial compartments

(EHMx, EHM, cytoplasm and tonoplast) using standard confocal microscopy. This has limited in-depth study of processes that take place at the haustorial interface.

Oomycetes of the genus *Phytophthora* are among the plant pathogens that form haustoria. A notorious member of the genus is the Irish potato famine pathogen *Phytophthora infestans*. Long after it triggered havoc in Europe in the mid-19th century, this hemibiotrophic pathogen remains a major threat to global food security as the most important disease of potato, an important food crop and calorie source for the world's poor (16,17). During host infection, *P. infestans* hyphae spread rapidly inside host tissue and penetrate multiple plant cells with digit-shaped haustoria before it sporulates and kills the infected plant tissue (18,19). Avrova et al. (18) showed that a haustoria-specific membrane protein PiHmp1 is required for full virulence validating the view that haustoria formation is critical for host colonization by *P. infestans*.

The mechanisms of EHM biogenesis in haustoriated plant cells, i.e. cells that are invaded by haustoria of *P. infestans* and other filamentous pathogens, are poorly understood. Curiously, several plant plasma membrane-localized proteins are excluded from haustorial interfaces indicating that the EHM is a distinct membrane compartment (12,20,21). In a first study of this type, Koh et al. (20) showed that eight Arabidopsis plasma membrane proteins are excluded from the EHM surrounding haustoria of powdery mildew fungi. Similarly, several plant plasma membrane-localized proteins are excluded from the EHM surrounding *P. infestans* haustoria in *Nicotiana benthamiana* but remorin REM1.3 and synaptotagmin SYT1 show a perihaustorial distribution (21,22). These differences in protein composition of the EHM relative to the plasma membrane are reminiscent of perimicrobial membrane compartments of host cells colonized by symbiotic arbuscular mycorrhizal fungi (23) and animal parasites (24,25). Several models have been proposed to account for selective protein exclusion from perimicrobial membranes such as the EHM. The EHM could be formed by plasma membrane invagination accompanied by secretory vesicle fusion at the haustorial neck followed by selective protein sorting (26,27). Alternatively, the EHM could arise by targeted secretion of various endomembrane compartments (12,28). The latter model appears more likely given that Lu et al. (21) observed significant reprogramming of vesicle trafficking in haustoriated plant cells that accommodate the oomycetes *P. infestans* and *Hyaloperonospora arabidopsidis*. In addition, Bozkurt et al. (22) showed that the plant membrane protein REM1.3 remorin accumulates in discrete EHM domains, suggesting that the EHM could be formed by multiple membrane microdomains.

One class of plant proteins that exhibits dynamic membrane trafficking during pathogen attack are cell surface pattern recognition receptors (PRRs), immune receptors that sense pathogen-associated molecular patterns (PAMPs) released from invading organisms (29–32). Classic plant PRRs include the extracellular leucine-rich repeat receptor-like kinases (LRR-RLKs) FLAGELLIN-SENSING 2 (FLS2) that recognize the bacterial PAMPs flagellin (33–35). To activate downstream signaling pathways, FLS2 requires BAK1 (also known as SERK3), another cell surface LRR-RLK, which serves as a co-receptor (36–38). BAK1 also functions as a regulatory protein for BRASSINOSTEROID-INSENSITIVE 1 (BRI1), a LRR-RLK involved in brassinosteroid hormone signaling that cycles between the plasma membrane and *trans*-Golgi network (TGN), and can be targeted to the vacuole for degradation via the late endosomes/multivesicular bodies pathway (39–41). Following activation by the flagellin-derived peptide flg22, FLS2 exhibits receptor-mediated endocytosis, and the spatiotemporal dynamics of endocytosis appear to be important for the steady state and function of the receptors (30,42). Cellular dynamics of PRR response to filamentous pathogens are unknown. However, similar to other integral membrane proteins, FLS2 is one of the membrane proteins that are excluded from the EHM surrounding *P. infestans* haustoria although the underlying mechanisms of this differential accumulation are unclear (21).

Endocytosis of activated plant PRRs, such as FLS2, occurs via the early endosome, late endosome, multivesicular body to vacuole pathway (referred to here as the late endocytic pathway) (29,32). As in other eukaryotes, this process and associated vesicle fusion events are regulated by Rab GTPases and SNARE proteins in plants. In animal systems, Rab5 and Rab7 GTPases regulate transition of early and late endosomes into multivesicular bodies and lysosomes during endocytosis (43). Consistent with this model,

ARA7, a Rab5 GTPase family member, localizes to both early and late endosomes (29), whereas RabG3c, a member of the Rab7 GTPase family, marks late endosomes and the tonoplast (44). Bottanelli et al. validated the late endosomal localization of Rab5 but concluded that the early endosome localization of Rab5 could be due to overexpression artifacts (45). In addition, it is believed that both early and late endosomes are probably multivesicular compartments; however, only the latter harbors vacuolar sorting receptors as cargo (46). Nonetheless, Rab GTPases can be useful markers to understand host–microbial interfaces. Recently, Lu et al. (21) reported that RabG3c is perihaustorial in plant cells infected by *P. infestans*, whereas the TGN marker VTI12 is excluded from the haustorial interface. These findings raise the possibility that trafficking from late endosomes to the EHM may take place (21).

Plant pathogens such as *P. infestans* deliver effector proteins inside plant cells to neutralize immune responses and enable parasitic infection (19,47). A well-studied class of host-translocated effectors is formed by the RXLR proteins secreted by plant pathogenic oomycetes during infection (13,48–50). RXLR effectors are probably delivered into host cells via haustoria (47,49). Heterologous expression of fluorescently tagged effectors in plant cells can be used to mark and trace host subcellular compartments in uninfected and infected tissue (13,22,51). Inside plant cells, RXLR effectors traffic to diverse subcellular compartments providing clues about their site of action and biological functions. Remarkably, two *P. infestans* RXLR effectors AVRblb2 and AVR2 focally accumulate around *P. infestans* haustoria when expressed inside *N. benthamiana* cells (19,52). Another RXLR effector, HaRXL17 from the downy mildew *H. arabidopsidis*, is also perihaustorial in infected *Arabidopsis thaliana* cells (15). These effectors have the potential to serve as useful molecular probes for plant cell biology (13,22,51). In this article, we developed AVRblb2 and HaRXL17 effectors as probes to discriminate between different perihaustorial compartments using live cell imaging, and investigate endomembrane trafficking at the haustorial interface. We discovered that the late endosome and tonoplast localized Rab 7 GTPase RabG3c is recruited to the EHM pointing to rerouting of vacuole-targeted late endosome trafficking to the haustorial interface. This process appears to be somewhat specific because a tonoplast-localized sucrose transporter was not detected at the EHM. Furthermore, we demonstrated the dynamic nature of this process by showing that, upon activation, the cell surface PRR FLS2 traffics to the host–pathogen interface. Our work provides insight into EHM biogenesis and reveals dynamic processes that recruit membrane compartments to a host–pathogen interface.

Results

Pathogen effectors as molecular probes that label distinct perihaustorial compartments

Several RXLR-type host-translocated oomycete effectors have been previously reported to localize around haustoria (15,19,52). We tested multiple combinations to determine whether these effectors could label distinct perihaustorial membrane compartments. Two effectors, AVRblb2 and HaRXL17, proved to be particularly useful and complementary. When co-expressed in *N. benthamiana* leaf epidermal cells, RFP fused to the effector domain of AVRblb2 without signal peptide and RXLR domain (RFP-AVRblb2) accumulated mainly at the plasma membrane, whereas GFP-HaRXL17 localized at both the plasma membrane and the tonoplast (Figure 1A). Next, we visualized the two proteins in epidermal *N. benthamiana* cells invaded by *P. infestans* haustoria (haustoriated plant cells) using the approach we described previously (19) (Figure 1B). Remarkably, the two proteins displayed non-overlapping peaks of fluorescence indicating that they accumulate in different compartments. Although RFP-AVRblb2 accumulated at the EHM, GFP-HaRXL17 was excluded from the haustorial interface and labeled the tonoplast, which is typically in close proximity to the EHM in *N. benthamiana* epidermal cells (Figure 1B). To better discriminate between the EHM and the tonoplast compartments using live cell imaging and confirm the differential localization, we slightly dehydrated the infected tissue to reduce the volume of the central vacuole (see *Materials and Methods* for details). This method resulted in a clear separation of perihaustorial compartments, namely the tonoplast, cytoplasm and the EHM, validating the finding that AVRblb2 and HaRXL17 distinctly label different compartments in both uninfected (Figure 1A and Figure S1A,B, Supporting Information) and haustoriated host cells (Figure S1C).

We used structured illumination microscopy (SIM) to further study AVRblb2 localization and confirm its presence at

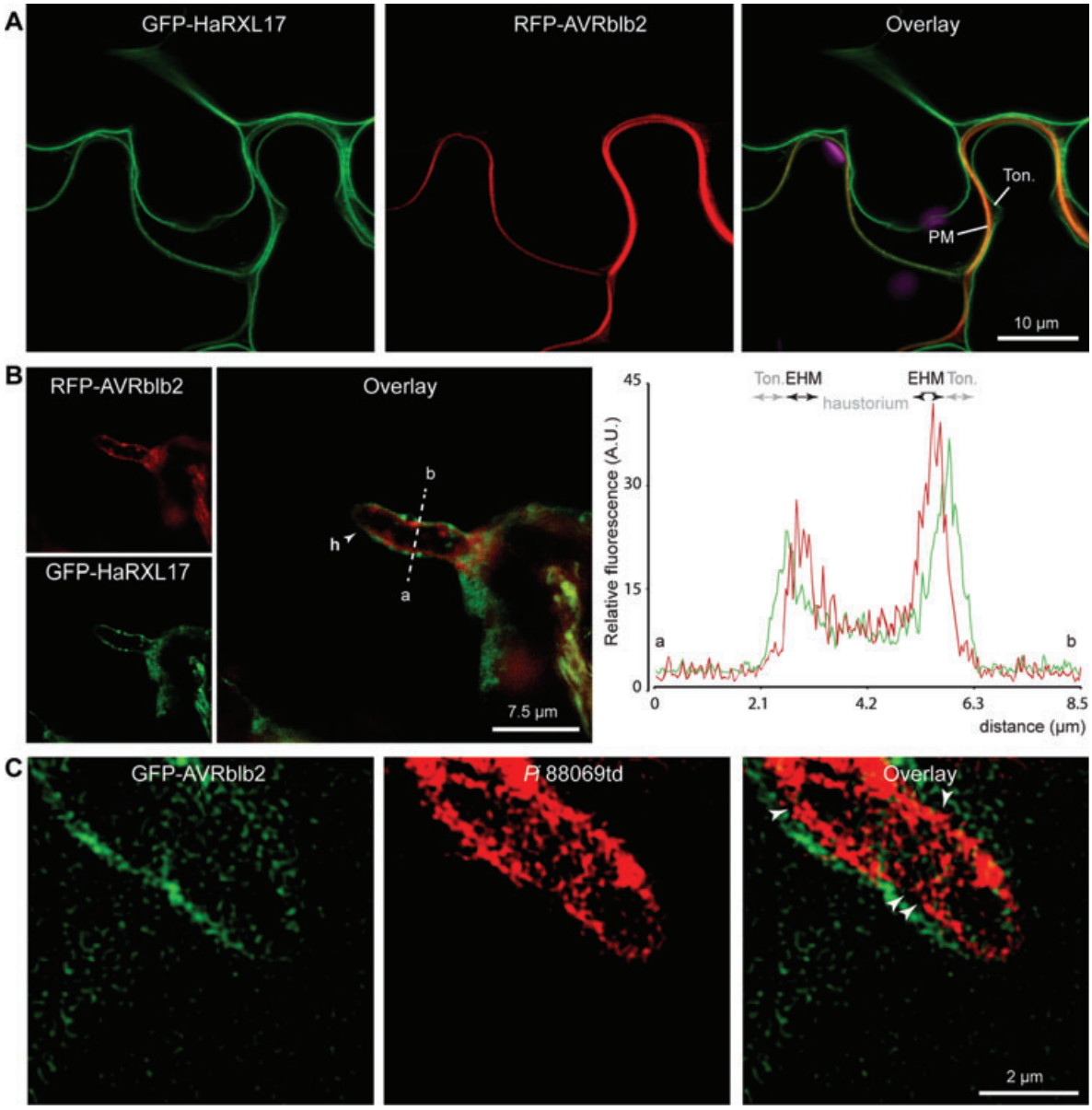

Figure 1: RXLR effectors as subcellular markers that label distinct perihaustorial compartments. A) Co-expression of GFP-HaRXL17 (left panel) and RFP-AVRblb2 (middle panel) in uninfected *N. benthamiana* leaf epidermal cells. GFP-HaRXL17 labeled the plasma membrane (PM) and tonoplast (Ton.), whereas RFP-AVRblb2 was localized at the PM. Two proteins only overlapped at the PM (right panel). Magenta marks plastids. B) Distribution of effector signals inside *P. infestans*-infected *N. benthamiana* cells. Both RFP-AVRblb2 (top left panel) and GFP-HaRXL17 (bottom left panel) showed perihaustorial localization; however, overlaid image indicates that only RFP-AVRblb2 labeled the EHM whereas GFP-HaRXL17 remained at the perihaustorial tonoplast (middle panel). Arrowhead points to haustoria (h). The fluorescence plot (right panel) shows relative fluorescence along the dotted line connecting points a and b as shown in the middle panel, highlighting tonoplast (Ton.) localization of GFP-HaRXL17 and EHM localization of RFP-AVRblb2. Arrowheads point to haustoria. C) SIM supports the EHM localization of AVRblb2. GFP-AVRblb2 signal surrounded haustoria of *P. infestans* 88069td (RFP-expressing strain). Measurements taken at the non-fluorescent gaps marked with arrowheads averaged at 212.5 $\pm$ 33 nm ($N = 4$), which is greater than *P. infestans* cell wall (50–100 nm), supporting the EHM localization of AVRblb2.

the EHM (Figure 1C). We used settings that enable at least two times higher resolution compared to confocal laser scanning microcopy. For these experiments, we expressed GFP-AVRblb2 in *N. benthamiana* and infected with a transgenic *P. infestans* strain (88069td, known as tdTomato) expressing the cytoplasmic red fluorescent marker tandem dimer RFP (49). SIM analysis of haustoriated cells revealed that GFP-AVRblb2 does not precisely trace the RFP signal from *P. infestans* haustoria. Rather, non-fluorescent gaps could be detected between the two signals indicating that GFP-AVRblb2 does not fill the space between the EHM and the pathogen haustorium (Figure 1C). The gaps between the GFP and RFP signals averaged 212.5 ± 33 nm ($N = 4$), which exceeds the width of the pathogen cell wall (50–100 nm) (11). These results are consistent with the conclusion reached using confocal laser scanning microcopy that AVRblb2 accumulates at the EHM (Figure S1B) (19). We conclude that AVRblb2 is unlikely to accumulate to high levels in the EHMx.

The late endosomal marker protein RabG3c (Rab7 GTPase family) traffics to the EHM

The late endosome marker protein RabG3c was previously shown to be perihaustorial in *P. infestans*-infected plant cells (21). This raises the hypothesis that RabG3c localization is perturbed during pathogen invasion possibly as a consequence of rerouting of the late endosome pathway toward haustoria. This prompted us to investigate whether late endosomes traffic to the EHM in haustoriated plant cells. Consistent with the reported late endosome localization of RabG3C (21), late endosomal marker RFP-ARA7 and YFP-AtRabG3c co-labeled punctate structures when co-expressed in *N. benthamiana* (Figure S2A). We then co-expressed RFP-AVRblb2 and YFP-AtRabG3c in uninfected *N. benthamiana* cells to more precisely determine the subcellular distribution of RabG3c (Figure S2B,C). As reported previously (44), YFP-AtRabG3c labeled predominantly the tonoplast (Figure S2B). These YFP-AtRabG3c signals did not colocalize with the plasma membrane-localized AVRblb2 (Figure S2B). Consistent with this interpretation, YFP-AtRabG3c remained associated with the tonoplast following salt-induced plasmolysis and labeled the 'bulb' structures, which typically form at the vacuolar membrane upon plasmolysis (Figure S2C). We did not detect any differences in the reported subcellular distribution of RabG3c in the presence of AVRblb2 indicating that the effector does not interfere with the localization of this plant protein (Figure S2B,C).

Next, we co-expressed RFP-AVRblb2 and YFP-AtRabG3c in *P. infestans*-infected *N. benthamiana* cells (Figure 2A). Both proteins showed marked accumulation around *P. infestans* haustoria (Figure 2A) as previously reported (19,21). However, this could be due to overlapping fluorescence signals emitted from closely associated perihaustorial compartments such as the tonoplast cytoplasm and EHM. To address this issue, we imaged cells in which the tonoplast and EHM are slightly parted away from each other (Figure 2B). Remarkably, we detected two peaks of YFP-AtRabG3c fluorescence around haustoria. In addition to labeling the tonoplast, YFP-AtRabG3c produced a signal at the EHM (52% of observations, $N = 43$) overlapping with the intensity peak signal produced by RFP-AVRblb2 (Figure 2B and Figure S2D). In the remainder of the cells (48%, $N = 43$), we observed either no signal or only a punctate distribution of YFP-AtRabG3c across the EHM compartments, unlike the systematic accumulation of AVRblb2 at the EHM (Figure S2E). These YFP-AtRabG3c marked endosomes did not overlap with the endomembrane compartments labeled by RFP-AVRblb2, indicating that these two proteins may use different pathways to reach the EHM (Figure 2C). In contrast, RabG3c endosomes displayed a significant overlap with endosomes labeled by the early and late endosomal marker protein RFP-ARA7 (Figure 2D) (31). Furthermore, consistent with Lu et al. results (21), which demonstrated that the TGN marker VTI12 is excluded from the haustorial interface, RFP-AtRabG3c did not colocalize with YFP-VTI12 (Figure S3). In conclusion, the presence of the late endosome marker protein RabG3c at the EHM and the detection of RabG3c-labeled late endosomes at the haustorial interface suggest that late endosomal trafficking is diverted toward haustoria in plant cells infected by *P. infestans*.

We performed additional experiments to determine the robustness of our observations. To assay endogenous *N. benthamiana* Rab7 proteins and rule out that RabG3c localization at the EHM is due to its expression via the *Cauliflower mosaic virus* (*CaMV*) 35S promoter, we set out to examine the subcellular distribution of a *N. benthamiana* RabG3c ortholog expressed through its native promoter. To achieve this, we first identified from

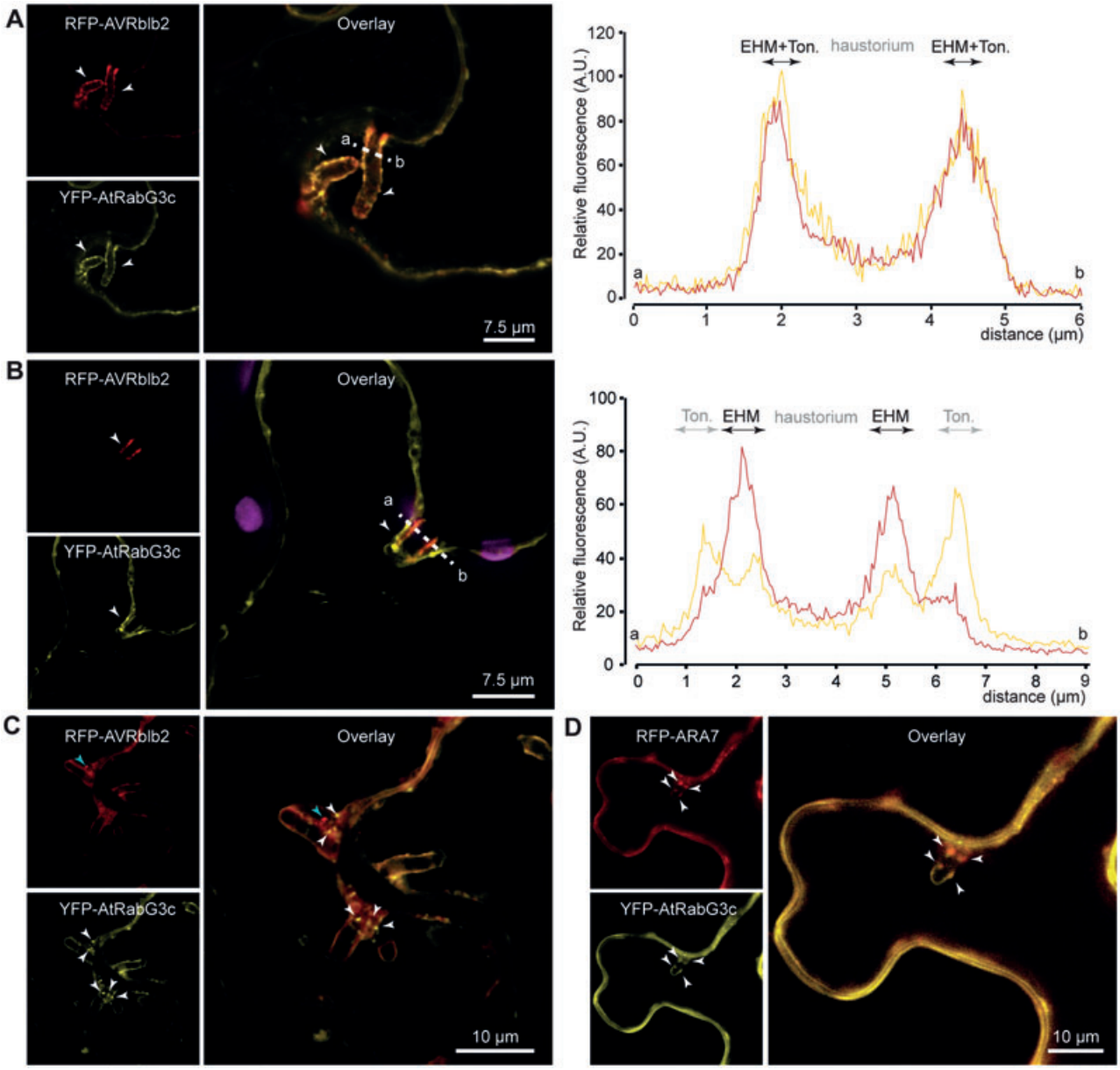

Figure 2: Late endosome marker protein RabG3c is recruited to the EHM compartments. A) Colocalization of YFP-AtRabG3c and RFP-AVRblb2 around *P. infestans* haustoria where tonoplast and EHM are tightly packed. The fluorescence plot (right panel) shows relative fluorescence along the dotted line connecting points a and b as shown in the middle panel reflecting converged signals at the tonoplast and the EHM. Arrowheads point to haustoria. B) Colocalization of YFP-AtRabG3c and RFP-AVRblb2 at the EHM in haustoriated cells where EHM and tonoplast are dispersed. Arrowhead points to ~~haustoria~~. The fluorescence plot (right panel) shows relative fluorescence along the dotted line connecting points a and b as shown in the middle panel, illustrating the EHM and tonoplast localization of YFP-AtRabG3c. Magenta marks plastids. C) RFP-AVRblb2 and YFP-AtRabG3c label different endomembrane compartments around haustoria. Teal arrowhead points to RFP-AVRblb2-labeled endomembrane compartments and white arrowheads point to YFP-AtRabG3c-labeled endosomes. D) YFP-RabG3c endosomes are also marked by RFP-ARA7. Arrowheads point to endosomes around haustoria where both proteins colocalize.

the *N. benthamiana* genome sequences of NbRabG3c-a and NbRabG3c-b, which show 88 and 90% amino acid sequence similarity to AtRabG3c, respectively, and appear to be the orthologs of the Arabidopsis protein (Figure S4A). Transient expression of 35S::GFP-NbRabG3c-a in *N. benthamiana* leaf epidermal cells revealed a similar endosome and tonoplast localization to AtRabG3c (Figure S4B,C), whereas 35S::GFP-NbRabG3c-b did not localize to the tonoplast, but labeled unknown endomembrane compartments (Figure S4D). Next, we investigated subcellular distribution of 35S::GFP-NbRabG3c-a in infected cells (Figure S4E). Also, in haustoriated cells, 35S::GFP-NbRabG3c-a displayed a similar subcellular distribution to YFP-AtRabG3c, accumulating around haustoria (Figure S4E) and at the EHM compartments (Figure 3A). Next, we replaced the *CaMV* 35S promoter with the NbRabG3c-a native promoter (707 bp upstream of start codon). In uninfected cells, co-expression of pRabG3c::GFP-NbRabG3c-a with RFP-AVRblb2 or RFP-ARA7 revealed pRabG3c::GFP-NbRabG3c-a fluorescence in endosomes marked by RFP-ARA7, but not RFP-AVRblb2, and tonoplast, although the fluorescence signal was weaker compared to the 35S::GFP:NbRAbG3c-a construct (Figure S4F,G). In *P. infestans*-infected cells, the pRabG3c::GFP-NbRabG3c-a construct yielded a perihaustorial localization pattern. In cases where the perihaustorial compartments could be separated, GFP-NbRabG3c-a labeled the tonoplast and RFP-AVRblb2-marked EHM compartments in 41% ($N = 24$) of the observations (Figure 3B,C and Figure S4H,I). In addition, in cases where the tonoplast is parted away from the EHM, we occasionally observed GFP-NbRabG3c-a-labeled endosomes across the EHM (Figure 3C and Figure S4H). As previously observed with AtRabG3c, the endosomal signal generated by the pRabG3c::GFP-NbRabG3c-a construct did not overlap with the RFP-AVRblb2 signal but overlapped with endosomes labeled by RFP-ARA7 (Figure 3C,D and Figure S4H,I). These results support our conclusion that late endosomes marked by the Rab7 proteins AtRabG3c and GFP-NbRabG3c-a are targeted to the EHM independently of the promoter or the protein used in the assays.

The tonoplast-localized protein SUC4 is not diverted toward the EHM

To determine whether RabG3c localization at the EHM reflects a transport route from vacuoles to the EHM compartments, we tested StSUC4, a potato ortholog of the Arabidopsis sucrose transporter AtSUC4 and a tonoplast-localized marker protein (53). Trafficking of AtSUC4 is known to follow the default vacuolar pathway, i.e. the endoplasmic reticulum-to-Golgi-to-tonoplast route (53). First, we co-expressed StSUC4-GFP fusion (Figure 4A) with either RFP-HaRXL17 or RFP-AVRblb2 in uninfected *N. benthamiana* epidermal cells (Figure 4B,C). StSUC4-GFP signal overlapped with RFP-HaRXL17 and was detected exclusively at the tonoplast, as previously reported for AtSUC4 (53). Then, we co-expressed StSUC4-GFP and RFP-AVRblb2, and imaged the two fusion proteins in haustoriated *N. benthamiana* cells (Figure 4D). Although StSUC4-GFP accumulated around haustoria consistent with its tonoplast localization, we failed to detect a GFP peak that overlaps with the EHM-localized RFP-AVRblb2 (100% of observations, $N = 10$) (Figure 4C,D). These results indicate that, unlike the late endosome and tonoplast protein RabG3c, SUC4 does not traffic to the EHM. Therefore, not all tonoplast-targeted proteins traffic to the haustorial interface, and the vacuolar-sorting pathway used by SUC4 is unlikely to be diverted to the EHM.

The endosomal protein BRI1 is recruited to EHM compartments

Our findings that RabG3c, but not SUC4, is diverted to the EHM suggest that rerouting may take place at the level of the late endosomes. To challenge this hypothesis, we tested additional proteins that localize to late endosomes. First, we tested whether the plasma membrane- and late endosome-resident receptor-like kinase BRI1 is also recruited to the haustorial interface. In uninfected plant cells, when co-expressed with RFP-AVRblb2, BRI1-GFP signals overlapped with RFP-AVRblb2 signals at the plasma membrane (Figure 5A). However, we also detected BRI1-GFP signal at endomembrane compartments (Figure 5A) as previously reported (54). These endosomal BRI1-GFP signals did not overlap with RFP-AVRblb2 signals (Figure 5A). In addition, we also detected a weak vacuolar BRI1-GFP signal, possibly owing to its transport from late endosomes to the vacuole (Figure 5A).

Next, we imaged BRI1-GFP in *P. infestans*-infected plant cells (Figure 5B–D). BRI1-GFP displayed a continuous

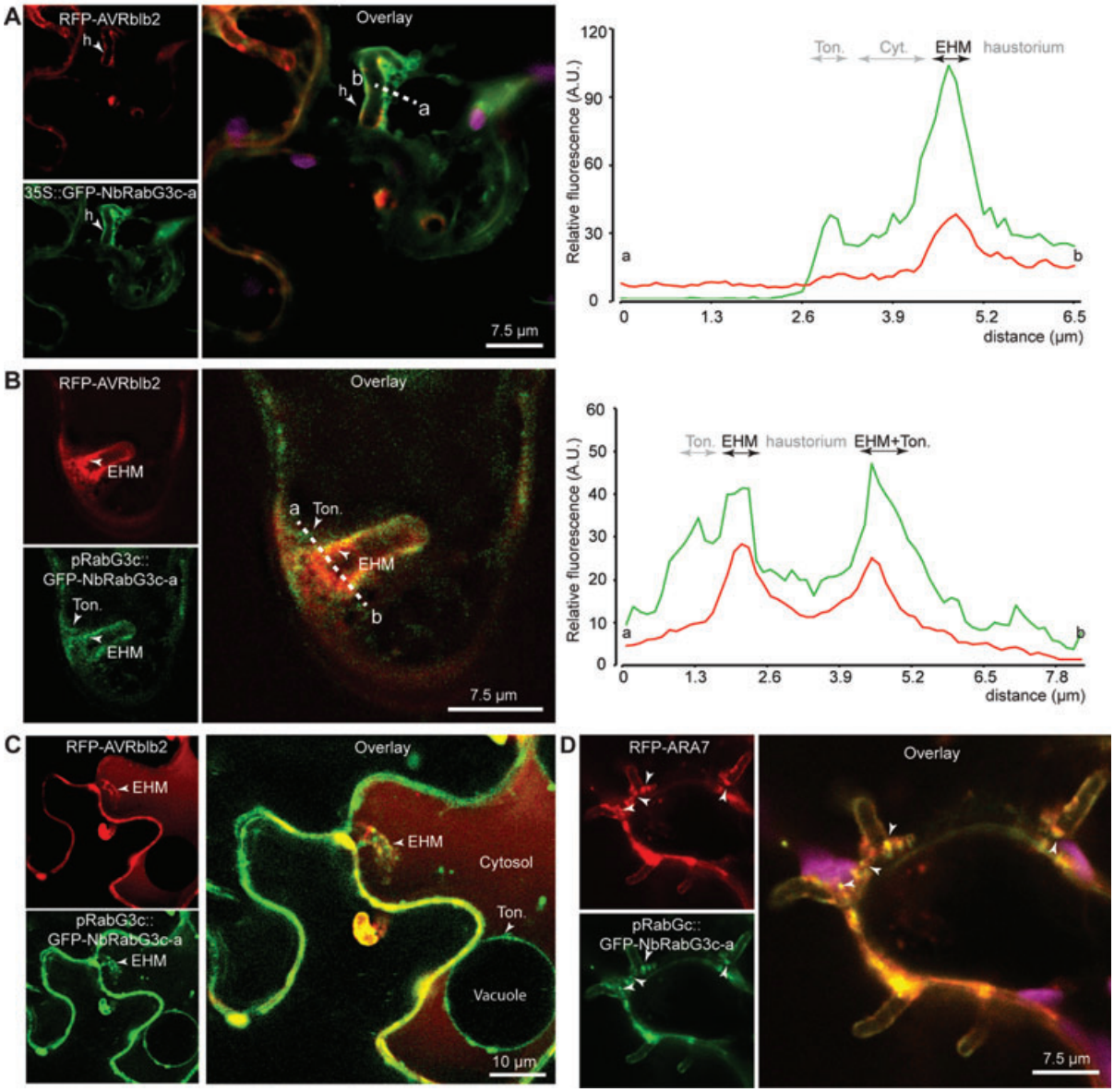

Figure 3: RabG3c is recruited to the EHM compartments when expressed either under 35S or its native promoter. A) Colocalization of 35S::GFP-NbRabG3c-a and RFP-AVRblb2 at the EHM. The fluorescence plot (right panel) shows relative fluorescence along the dotted line connecting points a and b as shown in the middle panel, highlighting the EHM and perihaustorial tonoplast localization of 35S::GFP-AtRabG3c-a (35S abbreviates *Cauliflower mosaic virus* 35S promoter). Arrowheads point to haustoria. B) Colocalization of pRabG3c::GFP-NbRabG3c-a and RFP-AVRblb2 at the EHM. pRabG3c::GFP-NbRabG3c-a signal was detected at both the tonoplast and the EHM. The fluorescence plot (right panel) shows relative fluorescence along the dotted line connecting points a and b as shown in the middle panel, highlighting the EHM and the tonoplast localization of pRabG3c::GFP-NbRabG3c. Arrowheads point to the tonoplast (Ton.) and EHM. C) EHM localization and endosomal distribution of pRabG3c::GFP-NbRabG3c-a at the EHM. Tonoplast, marked by pRabG3c::GFP-NbRabG3c-a and parted away from the EHM, was labeled by both pRabG3c::GFP-NbRabG3c-a and RFP-AVRblb2. pRabG3c::GFP-NbRabG3c-labeled endosomes across the EHM were not marked by RFP-AVRblb2. Arrowheads point to the tonoplast and EHM (h). Vacuole (Vac.) and cytoplasm (Cyt.) are also highlighted by absence or presence of weak RFP signal produced by RFP:AVRblb2 cytoplasmic pool. D) Colocalization of pRabG3c::GFP-NbRabG3c-a and RFP-ARA7 at endosomes around haustoria. Arrowheads point to the colocalization of both proteins at perihaustorial endosomes. Magenta marks plastids.

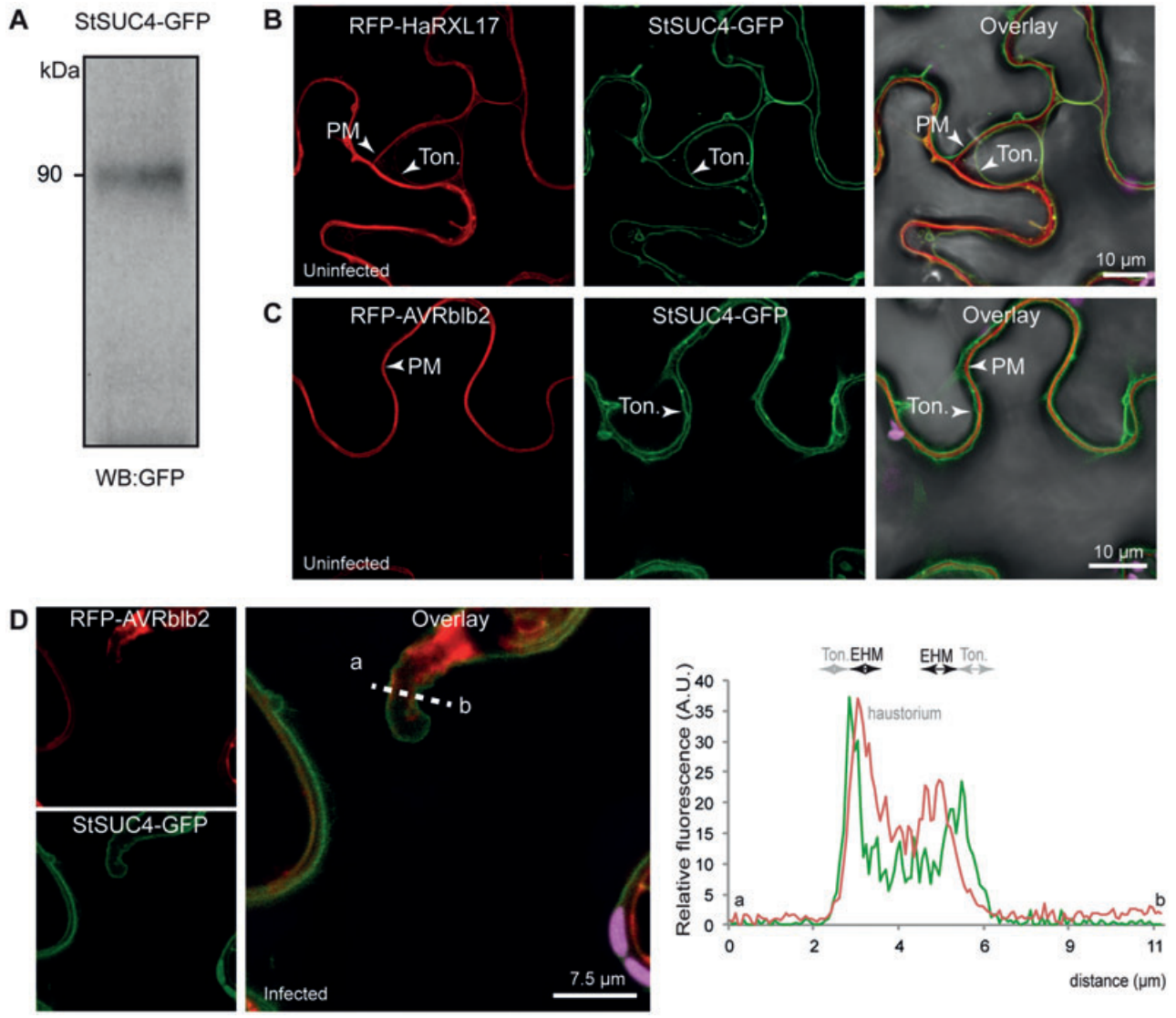

Figure 4: Not all vacuolar pathways are targeted to haustoria. A) Immunoblot representing stable expression of StSUC4-GFP in *N. benthamiana* leaf epidermal cells. B and C) Localization of StSUC4 at the tonoplast, co-expressed with RFP-HaRXL17 or RFP-AVRblb2. StSUC4-GFP and RFP-HaRXL17 colocalized at the tonoplast, whereas no overlap with StSUC4-GFP and RFP-AVRblb2 was observed. Arrowheads point to plasma membrane (PM) and the tonoplast (Ton.). D) Subcellular distribution of StSUC4-GFP inside *P. infestans*-infected *N. benthamiana* cells. Overlaid image demonstrates that StSUC4-GFP labels perihaustorial tonoplast but not the EHM marked by RFP-AVRblb2. The fluorescence plot (right panel) shows relative fluorescence along the dotted line connecting points a and b as shown in the middle panel, highlighting exclusion of StSUC4-GFP from the EHM. Magenta marks plastids.

fluorescence signal surrounding haustoria in 42% ($N = 129$) of the observations. This signal overlapped with the fluorescence produced by RFP-AVRblb2 or RFP-StREM1.3, a plant protein, which also marks the EHM (Figure 5B,C) (22). In addition to this observation, BRI1-GFP also labeled endosomal structures around haustoria in 60% ($N = 129$) of the observations (Figure 5D). In some cases (13/129), the BRI1-GFP-labeled endosomes accumulated around haustoria (Figure 5D). In summary, we conclude that the cell surface and endosomal receptor BRI1 traffics to EHM compartments unlike previously tested plasma membrane-localized receptors (21).

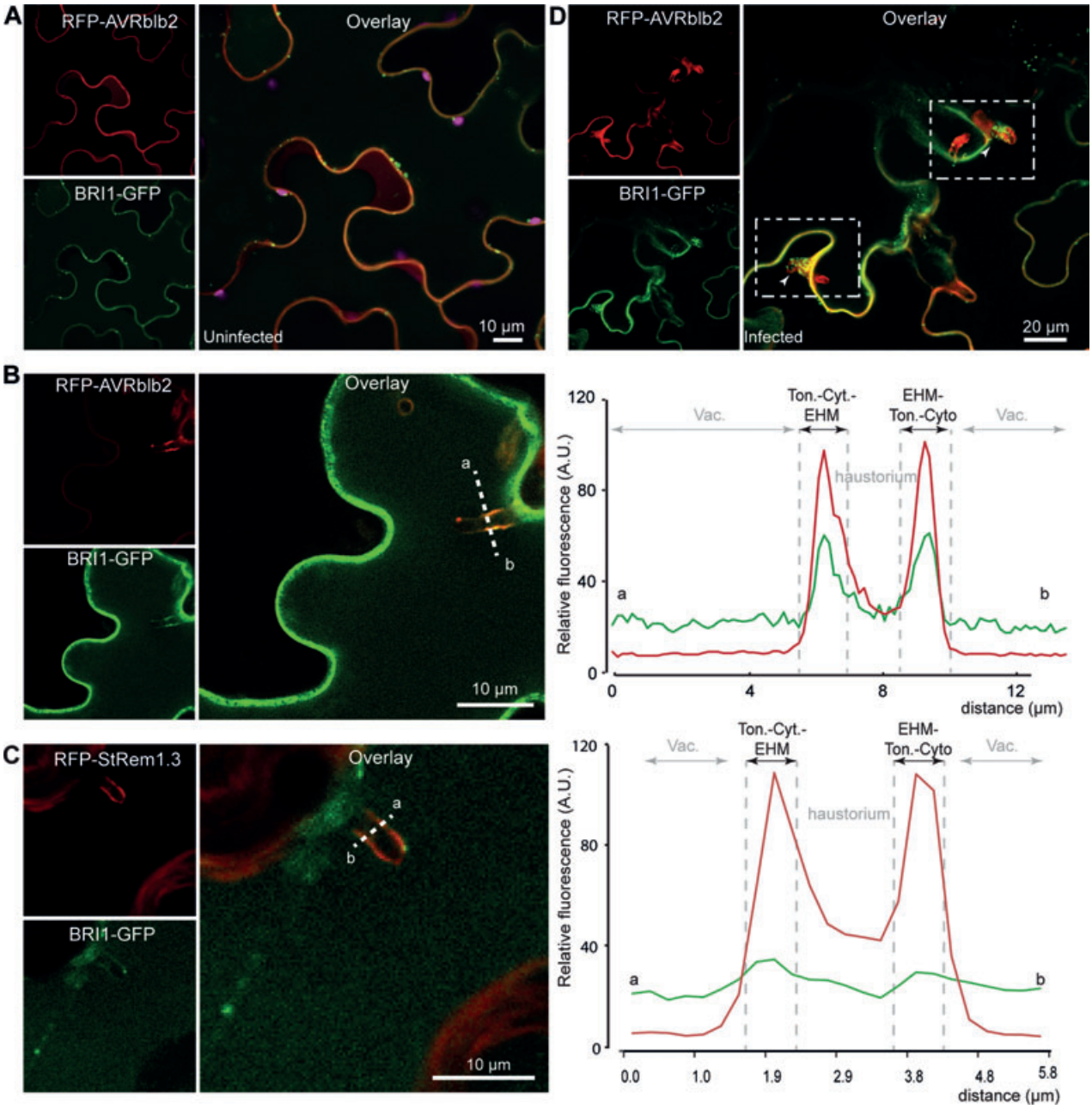

Figure 5: Late endosome cargo protein BRI1 traffics to the EHM compartments. A) BRI-GFP colocalized with RFP-AVRblb2 at the plasma membrane (PM) but not at endomembrane compartments. BRI1-GFP also showed weak vacuolar signal. Magenta marks plastids. B and C) Perihaustorial distribution of plasma membrane and late endosome localized BRI1-GFP around haustoria. When co-expressed with RFP-AVRblb2 or RFP-StREM1.3, BRI1-GFP signal was detected at perihaustorial endosomes and around haustoria and weakly at the vacuole. The fluorescence plots (right panel) show relative fluorescence along the dotted lines connecting points a and b as shown in the middle panels, highlighting perihaustorial localization of BRI-GFP at haustorial interface. D) Accumulation of BRI1-GFP-labeled endosomes around EHM compartments marked by RFP-AVRblb2. Arrowheads point to haustoria where BRI1-GFP endosomes accumulate.

The receptor kinase SERK3 (BAK1) is diverted to EHM compartments

Next, we tested the surface receptor-like kinase SERK3, which, similar to one of its co-receptors BRI1, localizes to late endosomes (54). Given that the well-studied Arabidopsis BAK1 elicits a cell death response in *N. benthamiana* (55), we cloned and used its potato ortholog StSERK3, which expressed stably in our assays when fused to GFP or RFP (Figure S5A). We first co-expressed StSERK3-GFP fusion protein with the perihaustorial markers RFP-HaRXL17 and RFP-AVRblb2 in uninfected *N. benthamiana* cells (Figure S5B,C). StSERK3-GFP signal overlapped with HaRXL17 and labeled plasma membrane, tonoplast and endomembrane compartments similar to Arabidopsis BAK1 (54). Then, we co-expressed StSERK3-GFP with RFP-AVRblb2 in *N. benthamiana* leaves, inoculated with *P. infestans* and imaged haustoriated plant cells (Figure 6A and Figure S5D,E). In all cases (>50 observed haustoria), StSERK3-GFP showed a perihaustorial distribution colocalizing with RFP-AVRblb2 (Figure S5D). To determine whether StSERK3-GFP perihaustorial localization is solely due to its accumulation in the tonoplast or whether it also reflects its presence at the EHM, we imaged haustoriated plant cells in which the tonoplast is parted away from the EHM. In such cells, we detected two peaks of StSERK3-GFP fluorescence around haustoria (Figure 6A). One of the two StSERK3-GFP peaks overlapped with the RFP-AVRblb2 signal (63%, $N = 8$) indicating that StSERK3 is diverted to the EHM (Figure 6A). Supporting this observation, StSERK3 occasionally displayed a punctuate distribution across EHM compartments (Figure S5E). Interestingly, in a haustoriated cell where the tonoplast and the EHM were slightly parted, the StSERK3-GFP signal emitted from these endomembrane compartments along the EHM did not overlap with RFP-AVRblb2 (Figure S5E), suggesting that these two proteins may use different pathways to reach the haustorial interface. In contrast, StSERK3-GFP-labeled endosomes were marked by late endosome marker YFP-AtRabG3c (Figure S5F). In addition, in these cells that co-express StSERK3-RFP and YFP-AtRabG3c, StSERK3-RFP produced a signal at both EHM compartments and tonoplast which overlapped with the YFP-AtRabG3c fluorescence (Figure S5F). These results indicate that both StSERK3 and AtRabG3c traffic to EHM compartments.

To further investigate the dynamics of StSERK3 recruitment at the EHM, we co-expressed StSERK3-GFP with the plant haustorial marker protein RFP-StREM1.3 in *P. infestans*-infected *N. benthamiana* cells (Figure 6B). In haustoriated plant cells where the perihaustorial compartments are parted away, we again detected StSERK3-GFP signal at the EHM compartments (marked by RFP-StREM1.3) in addition to the tonoplast (56%, $N = 16$) (Figure 6B). These findings further place SERK3 at the EHM during interactions between *P. infestans* and *N. benthamiana*.

The cell surface PRR FLS2 is excluded from the haustorial interface in plant cells invaded by *P. infestans* (21). To directly compare the localization of FLS2 with its co-receptor SERK3, we co-expressed FLS2-GFP with StSERK3-RFP in *P. infestans*-infected *N. benthamiana* cells (Figure S9). In cells where the tonoplast is separated from the EHM, StSERK3-RFP clearly marked both the EHM and tonoplast as previously noted. This localization sharply contrasted with FLS2-GFP, which was excluded from these compartments although both proteins could be detected at the plasma membrane (Figure 6C).

FLS2 is recruited to the haustorial interface upon activation by its peptide ligand flg22

Some of the activated plant cell surface receptors are known to undertake endocytosis using the late endocytic pathway (29–32). We hypothesized that the bacterial flagellin receptor FLS2 is absent from the haustorial interface between *N. benthamiana* and *P. infestans* (21) because it is inactive during interaction with an oomycete pathogen. According to this model, an activated FLS2 would then traffic to the haustorial interface. To test this hypothesis, we infiltrated solutions of the FLS2 peptide ligand flg22 into *P. infestans*-infected *N. benthamiana* leaves that co-express FLS2-GFP and RFP-AVRblb2, and performed live cell imaging (Figure 7). Upon flg22 infiltrations, we detected a significant perihaustorial FLS2-GFP signal, visualized either as endosomes or as a continuous distribution surrounding RFP-AVRblb2 marked haustoria, compared to water-treated samples (Figure 7A,B). We also observed greater than fourfold increase in number of haustoria that harbor FLS2-GFP-labeled endosomes in flg22-treated samples compared to water-treated control samples (Figure 7B). Similarly, upon flg22 treatments, we detected more than fivefold increase in cases where FLS2-GFP

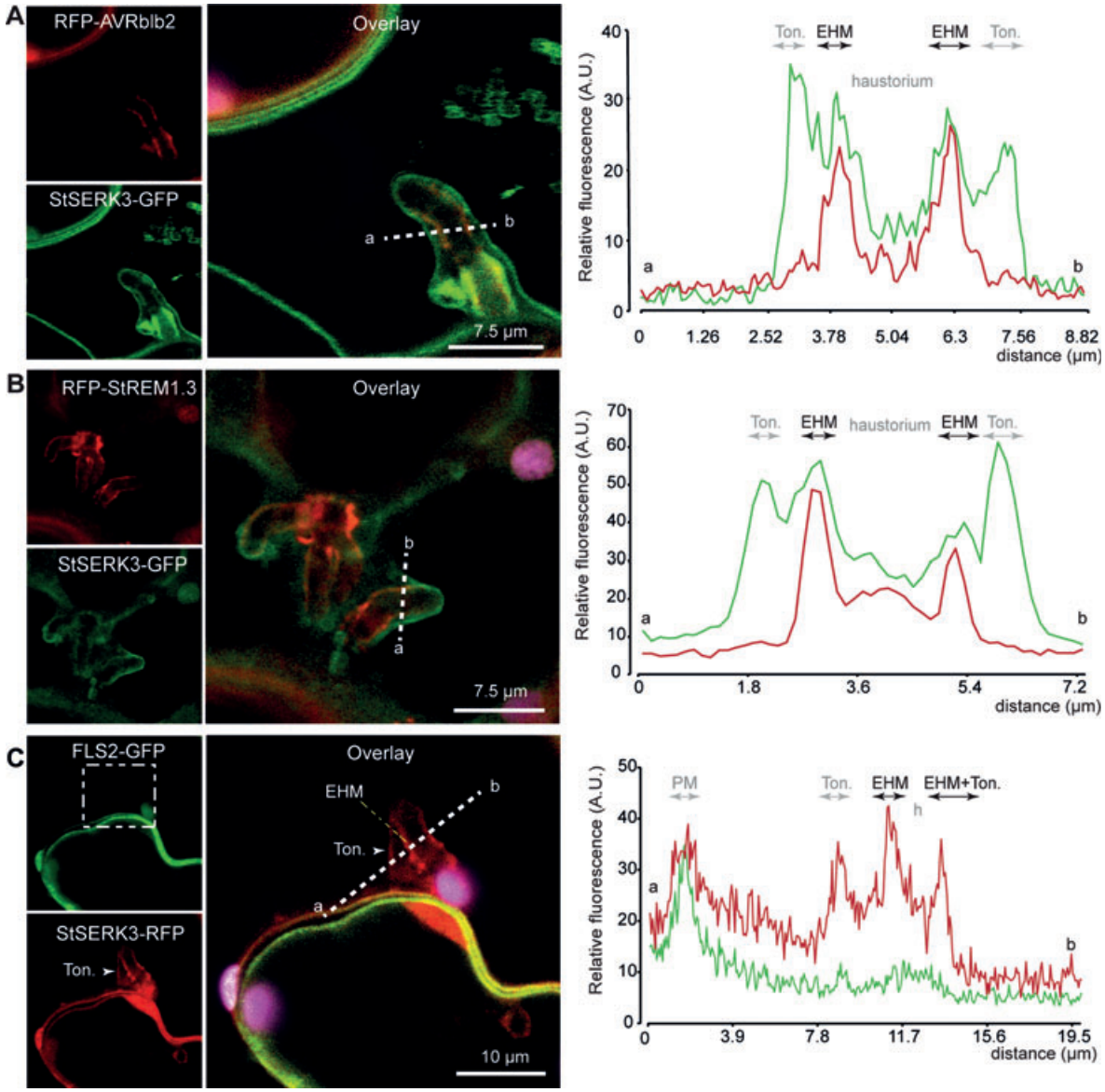

Figure 6: Late endosome cargo protein SERK3 traffics to EHM compartments. A) Colocalization of StSERK3-GFP and RFP-AVRblb2 at the EHM compartments inside infected plant cells. In host cells where perihaustorial compartments were separated, StSERK3-GFP showed a double-layered localization pattern enveloping haustoria, perihaustorial tonoplast and the EHM compartments, respectively. The fluorescence plot (right panel) shows relative fluorescence along the dotted line connecting points a and b as shown in the middle panel, illustrating the localization of StSERK3-GFP at the EHM compartments and the tonoplast. B) StSERK3-GFP colocalizes with plant protein StREM1.3 at the EHM. When co-expressed with RFP-StREM1.3, StSERK3-GFP labeled the EHM compartments and the tonoplast in haustoriated cells. The fluorescence plot (right panel) shows relative fluorescence along the dotted line connecting points a and b as shown in the middle panel, illustrating the localization of StSERK3-GFP at EHM compartments. C) Unlike FLS2-GFP, SERK3-RFP accumulates in EHM compartments. StSERK3-GFP co-expressed with FLS2-GFP, labeled both the tonoplast (Ton., shown by arrowhead) parted away from the EHM (indicated by the yellow line) and the EHM compartments. In contrast, FLS2-GFP was excluded from these compartments and was only detected at plasma membrane (PM). The fluorescence plot (right panel) shows relative fluorescence along the dotted line connecting points a and b as shown in the middle panel, highlighting the EHM compartment and the nearby tonoplast localization of StSERK3-RFP and exclusion of FLS2-GFP from these compartments. Magenta marks plastids.

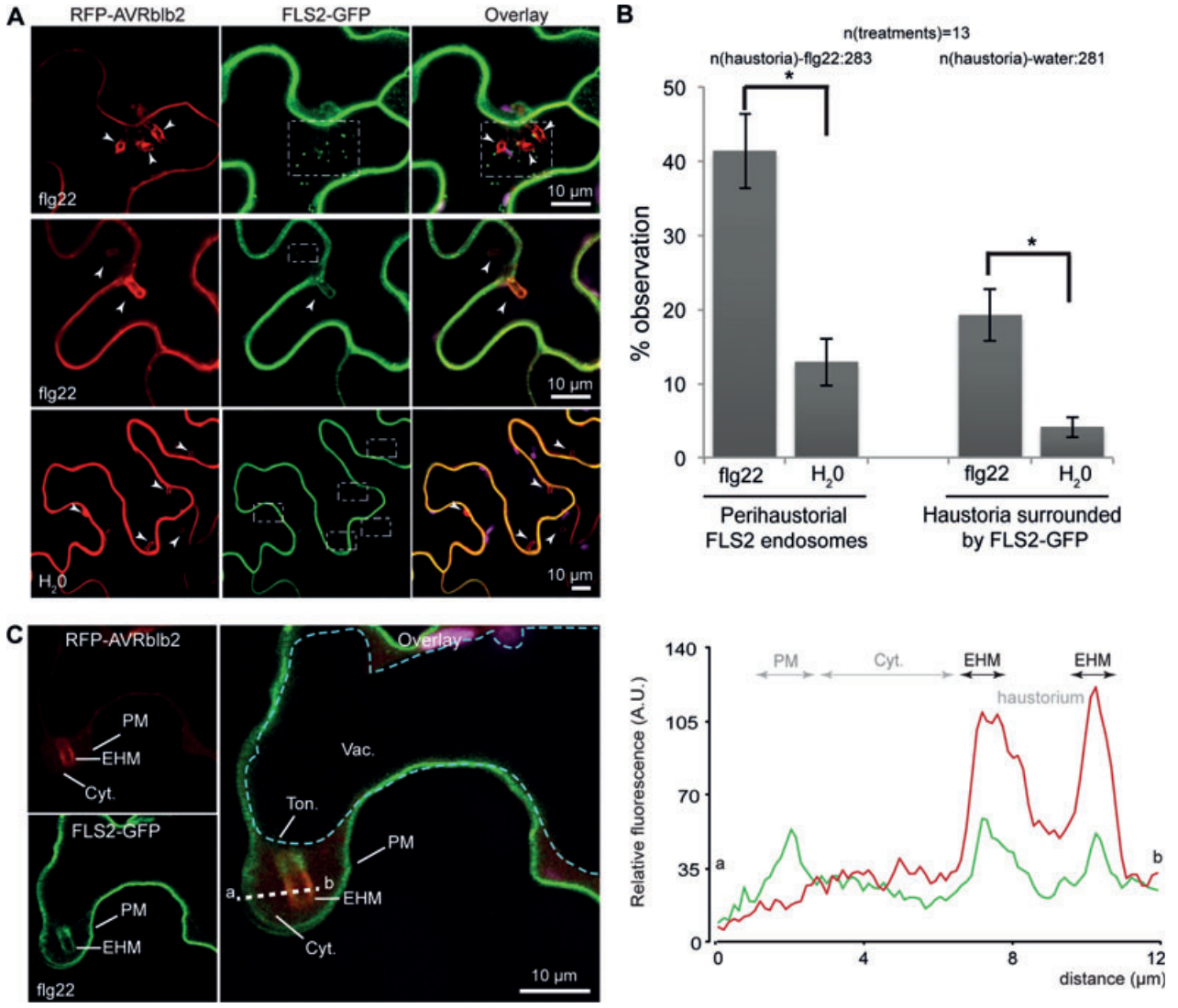

Figure 7: FLS2-GFP is recruited to the haustorial interface upon activation. A) FLS2-GFP was redirected to the haustorial interface when activated by leaf infiltration ~~with a~~ flg22 peptide solution. FLS2-GFP appeared at perihaustorial endosomes (top panel) or enveloped haustoria (middle left panel) upon activation by flg22 at a frequency significantly higher than in the water negative controls (lower panel). RFP-AVRblb2 was used to mark haustoria pointed by arrowheads. Dotted ~~squares~~ indicate haustoria, which are not enveloped by FLS2-GFP. Imaging was performed 1–4 h after infiltration of flg22 peptide. B) Quantification of FLS2-GFP distribution at the haustorial interface upon flg22 or water treatment in the presence of RFP-AVRblb2. An enhanced observation of FLS2-GFP signal either as endosomes or enveloping haustoria upon flgg22 treatment compared to the control water treatment. Quantification of haustoria is presented as percentage of average number of haustoria observed as enveloped by FLS2-GFP or overlapping with FLS2-GFP-labeled endosomes, for each independent experiment. Error bars represent standard error. *$p < 0.01$ (two-sample Mann–Whitney *U* test). C) In cells where tonoplast and EHM are parted away from each other, FLS2-GFP colocalized with RFP-AVRblb2 at the EHM compartments upon activation by flg22 treatment. The vacuolar membrane (tonoplast), which is shown by a teal-colored representative line, is parted away from the EHM compartments and the plasma membrane (PM) labeled by FLS2-GFP and RFP-AVRblb2. Cytoplasm (Cyt.) in between PM and large central vacuole (Vac.) was weakly labeled by RFP-AVRblb2. The fluorescence plot (right panel) shows relative fluorescence along the dotted line connecting points a and b as shown in the middle panel, highlighting localization of FLS2-GFP at the EHM compartments marked by RFP-AVRblb2. Magenta marks plastids.

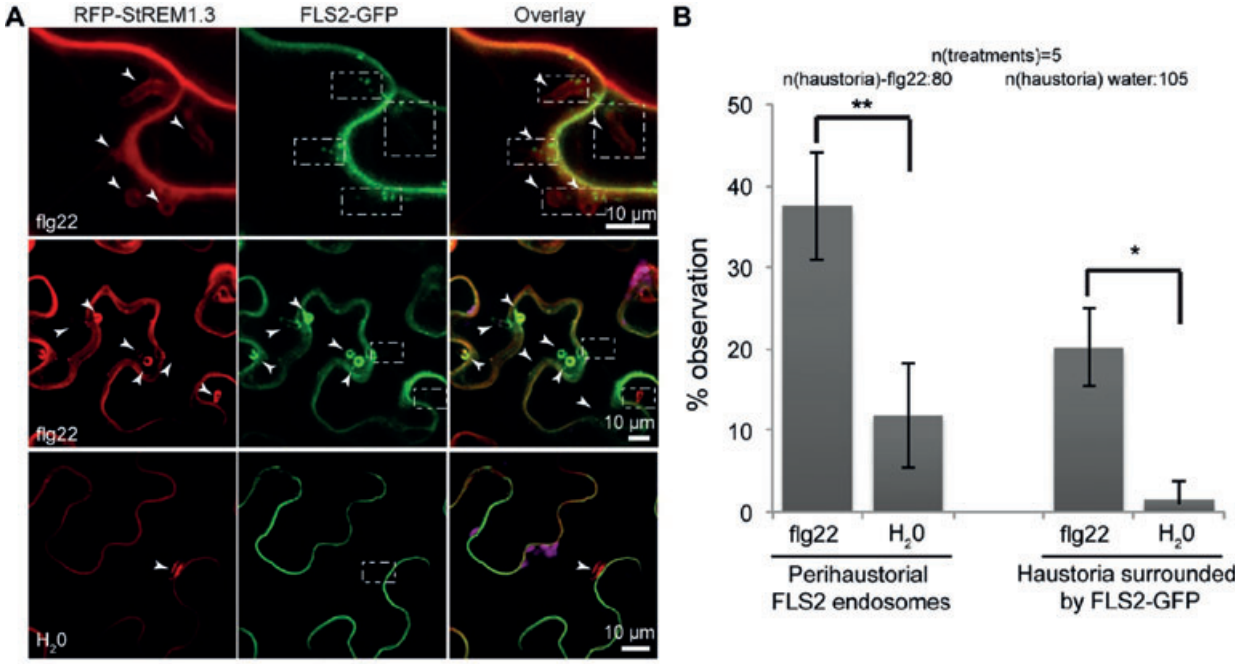

Figure 8: FLS2 colocalizes with StREM1.3 at the haustorial interface upon activation. A) Deployment of FLS2-GFP co-expressed with RFP-StREM1.3 to the haustorial interface when activated by flg22 treatment. Upon activation by infiltration with a flg22 peptide solution, FLS2-GFP signal either appeared at perihaustorial endosomes or enveloped haustoria (middle left panel), at a higher frequency than in the water treatment (lower left panel). Imaging was performed 1–4 h after infiltration of flg22 peptide. B) Quantification of FLS2-GFP recruitment to the haustorial interface marked by RFP-StREM1.3 upon activation. An increase in FLS2-GFP-labeled perihaustorial endosomes and FLS2-GFP-enveloped haustoria was noted upon flg22 treatments compared to the water control treatments. Quantifications were performed as explained in Figure 6B. *$p < 0.01$ indicates ~~significant~~ and **$p < 0.05$ indicates ~~highly~~ significant (two-sample Mann–Whitney *U* test). Magenta marks plastids.

enveloped haustoria (Figure 7B). We further investigated FLS2-GFP recruitment at EHM compartments in cells where the tonoplast and EHM are parted away (Figure 7C and Figure S6A). In flg22-treated tissue, we clearly detected an FLS2-GFP signal, which overlapped with RFP-AVRblb2 fluorescence (39%, $N = 46$) (Figure 7C) at the EHM compartments. In contrast, FLS2-GFP fluorescence peak at the RFP-AVRblb2-marked EHM was rarely observed in water-treated control samples (6%, $N = 35$) (Figure S6A). Overall, these results indicate that activation of the cell surface receptor FLS2 with its ligand flg22 results in a dynamic relocalization of this protein to the haustorial interface.

To independently validate these findings, we also investigated the dynamics of FLS2 haustorial transport using the plant EHM marker RFP-StREM1.3 (Figure 8A,B). As observed with AVRblb2, we noted more than threefold increase in the number of haustoria surrounded by FLS2-GFP endosomes, or greater than sixfold increase in the number of haustoria enveloped by FLS2-GFP, in samples infiltrated with the flg22 peptide relative to water-treated samples (Figure 8A,B). These results confirm our finding that activated FLS2 is recruited to the EHM compartments and further illustrate the dynamic nature of this process.

To investigate the identity of the FLS2-GFP-labeled endomembrane compartments that surround haustoria, we co-expressed RFP-AtRabG3c with FLS2-GFP in *P. infestans*-infected plant cells, and elicited the leaves with flg22 (Figure S6B,C). Interestingly, FLS2-GFP endosomes, which accumulate around haustoria upon flg22 treatment, showed a significant overlap with late endosomal marker RFP-AtRabG3c, indicating that activated FLS2 is

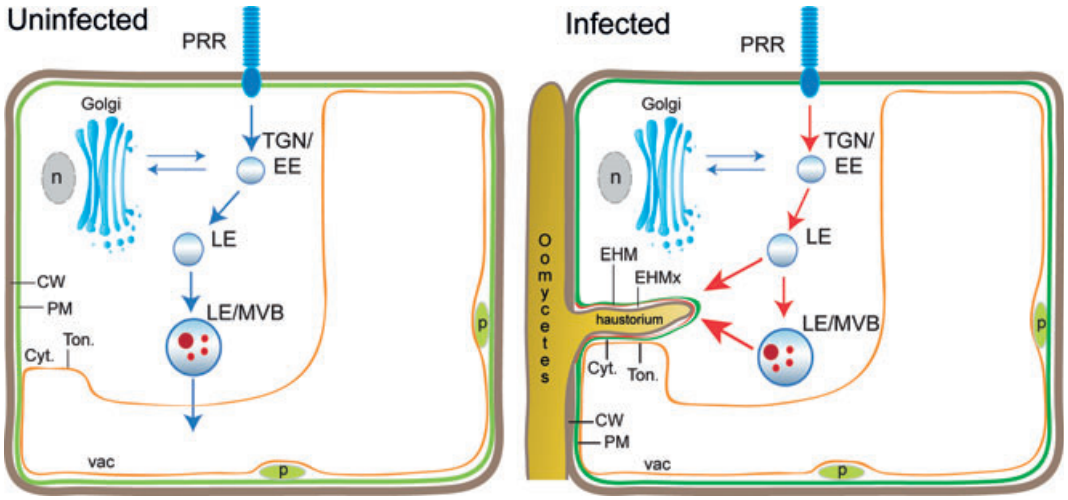

Figure 9: Rerouting of late endosomes to host–pathogen interface. Late endosomes, which recruit cargo from plasma membrane and TGN to the vacuole, are diverted toward haustoria. Upon activation, cell surface PRRs can be recruited at the host–pathogen interface via this route. EE: early endosome, LE: late endosome, TGN: trans-Golgi network, MVB: multi vesicular body, vac: vacuole, p: plastid, Cyt.: cytoplasm, PM: plasma membrane, n: nucleus, PRR: pattern recognition receptor, Ton.: tonoplast, EHM: extrahaustorial membrane, EHMx: extrahaustorial matrix.

internalized via the late endocytic pathway in haustoriated plant cells.

Discussion

Compared to animal systems, we know little about cellular dynamics during plant immune responses (5,56–60). In particular, processes such as regulation and perturbation of endomembrane trafficking by pathogens remain poorly understood. In this study, we used live cell imaging of fluorescently labeled pathogen and host proteins to dissect endomembrane trafficking processes at the haustorial interface in *N. benthamiana* cells infected by the Irish potato famine pathogen *P. infestans*. We found that late endocytic trafficking, which normally drives cargo proteins from the plant cell surface to the vacuole, is diverted toward the host–pathogen interface in infected (haustoriated) plant cells. Moreover, our results indicate that some surface receptors can be recruited to the haustorial interface upon activation. We propose a model in which some cell surface receptors that undergo ligand-induced endocytosis and traffic to late endosomes get sorted to host–pathogen interface, instead of taking the default route to the vacuole as in the case of uninfected cells (Figure 9). Rerouting of endocytic trafficking to the haustorial interface supports the view that regulation of vesicle trafficking is critical for accommodation of microbial structures inside host cells (12,19,23,28). Our study also sheds light on the EHM biogenesis. Although this membrane is continuous with the plasma membrane, the EHM appears to originate, at least in part, from redirection of endomembrane trafficking. This model accounts for the differences in protein composition between the plasma membrane and the EHM that have been noted in both fungal and oomycete pathosystems (12,20,21).

Pathogen-secreted effector proteins that accumulate at the host–pathogen interface have emerged as robust molecular probes to label specific subcellular compartments and define components of focal immunity (19,52). Here, we used oomycete effectors as cell biology markers to study vesicle trafficking processes at the haustorial interface, and subsequently discovered that a host endomembrane trafficking pathway is diverted to haustoria. Pathogen effectors distinctively labeled specific perihaustorial compartments and enabled the detection of these perihaustorial compartments using live cell imaging without further need of higher resolution techniques such as electron microscopy. Combined with the use of transient expression in the model plant *N. benthamiana* (61), this strategy enabled the

effective study of protein dynamics at the host–pathogen interface. It allowed rapid analyses of vesicle trafficking processes in haustoriated plant cells by, for instance, usage of multiple sets of fluorescently tagged proteins simultaneously. This should accelerate our understanding of plant cell autonomous immunity and the role of endomembrane trafficking in this process. It should be noted, however, that heterologous expression of effectors in plant cells may perturb host processes, and it is therefore critical to confirm any observation in the absence of co-expression with the effectors as we reported (Figures 6B,C and 8 and Figures S5C and S6B).

The Rab GTPase family plays a key role in eukaryotic endomembrane transport by determining target specificity for sorting endosomes to their destination (62). Eukaryotic cells contain multiple Rab GTPases that localize to distinct intracellular compartments. Members of the Rab7 class label late endosomes and mediate trafficking at the late endocytic pathway (43). The presence of RabG3c, a Rab7 protein, at the EHM indicates that late endosomes are diverted toward the EHM and reveals perturbation of host endomembrane trafficking during pathogen invasion. Recruitment of RabG3c at the host–pathogen interface is consistent with the observation that Rab7 coats perimicrobial plant–symbiont interfaces indicating that perturbation of late endosome trafficking might be a general process in plant–microbe interactions (63). Similarly, Rab7 labels animal lysosomal compartments that accommodate animal pathogenic bacteria (64,65). This points to similarities in pathogen accommodation processes between plants and animals, and further highlights the importance of reprogramming of vesicle trafficking during host–microbe interactions.

Transport of the Rab7 RabG3c toward haustoria appears to be under spatiotemporal regulation because RabG3c accumulation at the EHM was observed in 52% of the sampled haustoria (Figure 2B and Figure S2C). This contrasts to the effector AVRblb2, which is more consistently observed at the haustorial interface (19,22). What are the reasons behind the dynamic distribution of RabG3c at the EHM? Intrinsic properties of the protein or perturbations caused by the pathogen could explain the observed variation in EHM accumulation. It is possible that RabG3c is recruited to the EHM during certain stages of haustorial development or it may accumulate over time to reach detectable levels. For instance, RabG3c/late endosomes could traffic to the EHM compartments late during the biotrophic phase just before the switch to necrotrophy. Alternatively, host translocated effectors secreted by *P. infestans* may regulate RabG3c transport to the EHM. It is well known that animal pathogenic bacteria accommodated inside animal cells can deploy a variety of effector proteins to recycle Rab GTPases at the host–pathogen interface during different stages of infection (66). For instance, host-derived membranes enveloping the animal bacterial pathogen *Salmonella enterica* contain Rab5, whereas Rab7 is recruited at intermediate and late stages (67). Finally, similar to RabG3c, the plant membrane protein REM1.3 also shows dynamic localization around haustoria (22). Therefore, distribution of host proteins at the EHM appears to be a dynamic, and most likely complex and highly regulated process.

Dynamic recruitment of RabG3c to the EHM raises the question of whether late endosomes are diverted to haustoria or whether RabG3c is anchored to the EHM directly from its cytoplasmic pool. For instance, RabG3c could be recruited to the EHM by pathogen effectors to interfere with its function. However, we show that late endosome cargo proteins, including SERK3, are also recruited to the host–pathogen interface consistent with the view that it is the late endosomes that are diverted toward haustoria. In contrast, not all vacuolar transport pathways are redirected to the EHM because we did not detect EHM accumulation of a tonoplast-localized sucrose transporter, StSuc4, which uses a vacuolar pathway different from the late endosome pathway (53). Interestingly, as noted above, in contrast to the dynamic nature of RabG3c accumulation at the EHM, we consistently observed AVRblb2 at this interface. This suggests that these two proteins might use different trafficking pathways to reach the EHM. Indeed, perihaustorial endosomes marked by RabG3c did not overlap with endomembrane compartments marked by AVRblb2 (Figures 2C and 3C and Figures S2 and S4). Furthermore, analyses of the remorin REM1.3 in haustoriated plant cells revealed that the EHM is not uniform and is most likely formed by membrane microdomains (22). The emerging picture is that multiple vesicular pathways may converge toward the EHM to generate a

mosaic membrane interface between the host plant and the pathogen.

The presence of SERK3 at the *P. infestans*-induced EHM contrasts with the exclusion of plasma membrane-localized proteins such as FLS2 (21). Why is SERK3 present at the EHM? SERK3 could be recruited to late endosomes following various defense or growth-related stimuli independently of pathogen infection (Mbengue and Robatzek, personal communication). We also detected intracellular SERK3 signals in uninfected cells (Figure S6). In addition, it is possible that SERK3 is activated by cell surface receptors that respond to PAMPs released from *P. infestans*, leading to its recruitment to late endosomes and diversion to the EHM. In agreement with this, INF1 elicitin, a PAMP-like protein, secreted by *P. infestans* requires SERK3 to activate cell death and immunity in tobacco leaves (55). In contrast, there is no evidence that FLS2, a receptor for bacterial flagellin, is activated and subsequently internalized into late endosomes during infection by *P. infestans* (Figure 9). Hence, it is excluded from the EHM in host cells infected with *P. infestans* haustoria but is recruited to the haustorial interface when activated by external flg22 stimulus (Figure 7). Intriguingly, FLS2 was reported to display a perihaustorial distribution in *A. thaliana* cells infected with haustoria of the oomycete downy mildew *H. arabidopsidis* (21). Whether this is due to differences in EHM biogenesis between the two host–pathogen systems or whether FLS2 has different activation dynamics during infection by *H. arabidopsidis* remains to be addressed.

Our finding that a cell surface receptor is recruited to the haustorial interface upon activation could be a consequence of the general rerouting of the late endocytic pathway. Alternatively, the redeployment of activated PRRs to the EHM may bear some functional significance. A critical question is the extent to which redeployed cell surface receptors are able to initiate immune signaling from the EHM. Initially, receptor-mediated endocytosis was thought to downregulate signaling by reducing receptor levels at the cell surface and enabling receptor recycling (68). However, in animal cells accumulating evidence points to more complex functions, including modulation of signaling at endosomal compartments (68). For instance, the late endosome compartment, initially thought to attenuate signaling by sorting the surface receptors to the vacuole for degradation, can also mediate specific signaling events such as proinflammatory signaling in macrophages or growth and development in animal cells (68–72). The role of receptor-mediated endocytosis may turn out to be equally complex in plants. Redeployment of the late endocytic pathway toward haustoria could contribute to the plant immune response to pathogen penetration. This process could function in recruiting defense and signaling components to the pathogen contact sites. Consistent with this view, Nielsen et al. (73) reported that GNOM, a plant-specific regulator of Rab GTPase activity, is required for Arabidopsis penetration resistance and deposition of defense compounds at encasements around powdery mildew haustoria. However, in the case of the *N. benthamiana–P. infestans* system, haustoria are rarely encased (19), and the processes we are visualizing in haustoriated cells reflect a susceptibility state that is favorable to the pathogen. Thus, it is perhaps more likely that pathogens redirect the late endocytic pathway to the haustorial interface for their own benefits, e.g. to diminish late endosome signaling or to prevent receptor recycling. Future studies are required to uncover the degree to which rerouting of the late endocytic pathway plays a role beyond EHM biogenesis.

Materials and Methods

Biological material

Nicotiana benthamiana plants were grown and maintained throughout the experiments in a greenhouse with controlled temperature of 22–25°C and high light intensity. Growth of *P. infestans* isolates and inoculation assays were performed as described elsewhere (74,75). In brief, *P. infestans* cultures were grown in pates with rye sucrose agar (RSA) for 12–14 days. Sporangia were harvested from plates using cold water and zoospores were collected after 2–3 h of incubation at 4°C. Infection assays were performed by droplet inoculations of *P. infestans* zoospore solutions on detached *N. benthamiana* leaves as described earlier. For all infection assays, we used *P. infestans* isolate 88069 or 88609td, a transgenic strain of this isolate expressing the red fluorescent marker tandem dimer RFP [known as tdTomato (49)].

Sequence analysis

To identify putative orthologs of *A. thaliana* AtRabG3c in *N. benthamiana* genome we performed a BLASTP (76) search against *N. benthamiana* proteome using as query the protein sequence AtRabG3c. We found two protein hits: NbS00011851g0008.1 and

NbS00011545g0023.1. To verify the gene calls and open reading frame predictions of the two putative orthologs NbS00011851g0008.1 and NbS00011545g0023.1, we performed a TBLASTN search against the *N. benthamiana* scaffolds and used the flanking regions to design specific primers (NbRabG3cA_F_TB and NbRabG3cA_R_TB; NbRabG3cB_F_TB and NbRabG3cB_R_TB). (In Table S1, we corrected the ORF prediction of NbS00011545g0023.1 with the sequence of the amplicon obtained from *N. benthamiana* cDNA (GenBank submission ID 1712651).] We renamed the genes NbS00011851g0008.1 and NbS00011545g0023.1 to NbRabG3c-a and NbRabG3c-b, respectively. The Clustal X program was used for multiple sequence alignments of AtRabG3c and the two orthologs NbRabG3c-a and NbRabG3c-b (77). Boxshade (http://sourceforge.net/projects/boxshade/) was used to visualize the sequence alignment in ASCII differences format.

Molecular cloning and plasmids

Various constructs used in this study were previously published as follows: RFP- AVRblb2 and GFP-AVRblb2 constructs were previously described by Bozkurt et al. (19), GFP-HaRXL17 and RFP-HaRXL17 constructs by Caillaud et al. (15), RFP-StREM1.3 construct by Bozkurt et al. (22), YFP-VTI12 by Lu et al. (21), FLS2-GFP and RFP-ARA7 constructs by Beck et al. (29), ER-RFP construct by Nelson et al. (78) and YFP-AtRabG3c (wave11) construct by Geldner et al. (44). The 35S::GFP-NbRabG3c-a and the 35S::GFP-NbRabG3c-b constructs were generated by PCR amplification from *N. benthamiana* cDNAs using primer pairs NbRabG3cA_F_TB and NbRabG3cA_R_TB, as well as NbRabG3cB_F_TB and NbRabG3cB_R_TB, followed by Gateway cloning into the pENTR/D/TOPO (Invitrogen) entry clone then into the destination vector, the pK7WGF2 (79). pRabG3c::GFP-NbRabG3c-a construct was generated by replacing the CaMV 35S promoter of 35S::GFP-NbRabG3c-a with a 707-bp region upstream of NbRabG3c-a by digestion with restriction enzymes *SacI* and *SpeI*. The 707-bp fragment was amplified from *N. benthamiana* genomic DNA with a forward primer including SacI restriction site and reverse primer including a SpeI restriction site (NbRabG3c_pro_F_TB and NbRabG3c_pro_R_TB, Table S1). StSUC4-GFP constructs were generated by PCR amplification from *Solanum tuberosum* cDNA using primers StSUC4_F_TB and StSUC4_R_TB followed by Gateway cloning into the entry vector pENTR/D/TOPO (Invitrogen) then into the pK7FWG2 (GFP) and pB7RWG2 (RFP) vectors, respectively (79). The potato ortholog of AtSERK3/BAK1 was cloned using previously reported primers developed for *N. benthamiana* NbSERK3/BAK1 (55). A 1848-bp fragment was amplified from *S. tuberosum* cv. Désirée cDNA using Phusion proof reading polymerase (New England Biolabs). The PCR product was first introduced into pCRII-BLUNT/Topo (Invitrogen) then into the binary GATEWAY destination vector pK7WGF2 (GFP) (79). The obtained ortholog sequence was named StSERK3 (GenBank accession number KJ625629). The StSERK3 protein showed a conserved domain structure with the previously characterized AtSERK3/BAK1 with 84% similarity. StSERK3 was more similar to *N. benthamiana* orthologs NbSERK3A/B (95%) than to AtSERK3/BAK1. We used StSERK3 sequence as query to search against the potato proteome and identified three putative homologs: PGSC0003DMP400030908, PGSC0003DMP400047883 and PGSC0003DMP400047882. StSERK3 shared the highest similarity to PGSC0003DMP400030908 in amino acid sequence. PGSC0003DMP400030908-predicted protein was mis-annotated in the potato genome (80) as it lacks the first 90 amino acid compared to StSERK3. Primers described in cloning of the constructs are listed in Table S1.

Transient gene-expression assays in *N. benthamiana*

Agrobacterium tumefaciens-mediated transient gene expression (agroinfiltration) in *N. benthamiana* leaf epidermal cells was used in all experiments (81). In brief, we used *A. tumefaciens* GV3101 strain to deliver T-DNA constructs into 3- to 4-week-old *N. benthamiana* plants. Overnight *A. tumefaciens* cultures were harvested by centrifugation at 1000×***g*** and resuspended in agroinfiltration medium [10 mM $MgCl_2$ and 5 mM 2-(*N*-morpholine)-ethanesulfonic acid (MES), pH 5.6] prior to syringe infiltration into *N. benthamiana* leaves. For each of the *A. tumefaciens* strain-containing different constructs, a final OD_{600} of 0.3 was used. For all of the transient co-expression assays, each *A. tumefaciens* strain carrying a plant expression construct was mixed in a 1:1 ratio in agroinfiltration medium to a final OD_{600} of 0.4–0.6. For transient protein expression followed by *P. infestans* inoculation, the constructs were infiltrated as described above and *P. infestans* was inoculated between 4 and 24 h later (19).

Confocal and structured illumination microscopy

All microscopy analyses were performed on *N. benthamiana* epidermal cells 2–4 days after agroinfiltration. Patches of *N. benthamiana* leaves were cut and mounted in water and analyzed on a Leica TCS SP5 confocal microscope (Leica Microsystems) using 63× water immersion objective. Specific excitation wavelengths and filters for emission spectra were set as described earlier (21). Dehydration of plant epidermal cells was occasionally observed in *P. infestans*-infected samples during confocal laser scanning microscopy sessions and yielded a slight separation between the EHM and tonoplast. We took advantage of this and increased the frequency of such occurrences by briefly exposing the cut leaf patches to air for 10–30 min before microscopy. To avoid bleed-through from different fluorophores, colocalization images were taken using sequential scanning between lines and acquired using multichannels. Image analysis was performed using the Leica LAS AF software, ImageJ (1.43u) and Adobe Photoshop CS6. The super resolution images were taken on a Zeiss Elyra PS1 structured illumination microscope (SIM) using 63× oil immersion objective (22). The GFP and RFP probes were excited using 488 and 561 nm laser diodes and their fluorescent emissions collected at 495–550 and 570–620 nm, respectively. To generate a single 3D-SIM image, 15 raw images were collected (five phases and three rotations) and processed using Zeiss Zen Black software. The GFP and RFP were sequentially collected and the SIM images were color aligned using the channel alignment tool in Zen (calibration beads were taken at the end of an experiment and used to generate an alignment matrix).

Western blot analyses

Proteins were transiently expressed by *A. tumefaciens*-mediated transient expression (agroinfiltration) in *N. benthamiana* leaves and harvested 3 days after infiltration. Protein extractions and western blot analyses were performed as described elsewhere (82). For protein extraction of StSUC4-GFP, leaf tissue was grinded in liquid nitrogen followed by 3–5 min room temperature incubation with SDS protein loading dye. Commercial anti-GFP (Invitrogen) and anti-RFP (Invitrogen) antibodies were used as primary antibodies.

RT-PCR assays

Total RNA (10 mg) was extracted from 4-week-old *N. benthamiana* leaves using the RNAeasy Plant Mini Kit (Qiagen). They were subjected to DNase I treatment (Ambion) according to the manufacturer's protocol. Two micrograms of DNase-treated RNA was reverse transcribed with the Ominiscript RT Kit (Qiagen) to produce cDNA.

FLS2 activation assays

The FLS2 peptide ligand (flagellin or flg22) was purchased from EZBiolabs. For the FLS2 activation assays, flg22 was diluted to a concentration of 100 μM for final use (32). Flg22 or water control was infiltrated into *P. infestans*-infected leaf patches that express the FLS2-GFP construct at least 1 h before imaging (i.e. imaging was performed 1–4 h after infiltration of flg22 peptide).

Statistical analyses

Quantification of FLS2 activation around haustoria was performed by counting perihaustorial FLS2 distribution. The number of haustoria observed, which either were enveloped by FLS2-GFP fluorescence or accommodated FLS2-GFP endosomes, was assessed for flg22 or water control treatments. The average number of haustorial observations made for each treatment was plotted in percentage. Significance of the differences observed was assessed by mean of a two-sample Mann–Whitney *U* statistical test (using unpaired as measurements were not in matching pairs) as implemented in R package (83). Measurements were significant when $p < 0.01$ and highly significant when $p < 0.05$.

Acknowledgments

We thank Sebastian Schornack, Silke Robatzek, Martina Beck, Malick Mbengue, Ben Petre and Cyril Zipfel for useful suggestions. We are grateful to Marie-Cecile Caillaud and Jonathan D. G. Jones for useful comments and providing the GFP/RFP-HaRXL17 constructs, to Markus Albert for providing the BRI1-GFP construct and to Stephen Whisson for providing *P. infestans* 88069td strain. We thank Grant Calder for technical help with SIM.

Supporting Information

Additional Supporting Information may be found in the online version of this article:

Figure S1: AVRblb2 effector marks the extrahaustorial membrane. A) Subcellular distributions of co-expressed oomycete effectors GFP-HaRXL17 and RFP-AVRblb2 in uninfected cells where the tonoplast (Ton.) and plasma membrane (PM) are parted away and the cytoplasm (Cyt.) is no longer a thin layer between the two membranes. GFP-HaRXL17 labeled the PM and Ton., whereas AVRblb2 labeled only the PM. In addition, although RFP-AVRbl2 was predominantly at the PM, it showed a weak cytoplasmic signal that reaches detectable levels in some cases possibly due to *in planta* cleavage of the fusion protein. B) Western blot of RFP-AVRblb2 indicating weak *in planta* cleavage of fusion protein. C) Localization of GFP-HaRXL17 and RFP-AVRblb2 in haustoriated cells, where perihaustorial tonoplast is separated from the EHM. These experiments further show that, unlike RFP-AVRblb2, GFP-HaRXL17 is excluded from EHM compartments. Magenta marks plastids.

Figure S2: RabG3c is recruited to the EHM in a dynamic fashion. A) RabG3C colocalizes with the late endosome marker protein ARA7. B and C) RFP-AVRblb2 does not alter previously reported subcellular distribution YFP-AtRabG3c (44). B) No overlap between the fusion proteins was observed; YFP-AtRabG3c was detected at the tonoplast and RFP-AVRblb2 at plasma membrane (PM). C) Salt-induced plasmolysis of *N. benthamiana* cells expressing YFP-AtRabG3c and RFP-AVRblb2 validates tonoplast localization of YFP-AtRabG3c. Arrowheads point to bulbs, structures that occur along the vacuolar membrane upon plasmolysis. ~~C~~) and ~~D~~) Dynamic nature of YFP-AtRabG3c recruitment to the EHM marked by RFP-AVRblb2. YFP-AtRabG3c was detected at the EHM in 52% of the cases where the tonoplast and the EHM are parted away, whereas it remained excluded from the EHM in the remainder. The fluorescence plots (right panel) show relative fluorescence along the dotted line connecting points a and b as shown in the middle panels, highlighting (~~C~~) recruitment or (~~D~~) exclusion of YFP-AtRabG3c at the EHM. White and teal arrowheads point to the EHM and late endosome across the EHM compartments, respectively. Magenta marks plastids.

Figure S3: RabG3c does not colocalize with the TGN marker VTI12. A and B) RFP-AtRabG3c-labeled endosomes do not overlap with the TGN marker YFP-VTI12. C) Co-expression of RFP-AtRabG3c with the RFP empty vector construct.

Figure S4: NbRabG3c-a traffics EHM compartments when expressed by using its native promoter. A) Protein sequence alignments of homologs of *A. thaliana* RabG3c from *N. benthamiana* NbRabG3c-a (NbS00011851g0008.1) and NbRabG3c-b (corrected gene model for NbS00011545g0023.1). Yellow boxes indicate the positions of sequence motifs that are conserved in Rab GTPases and are involved in nucleotide binding and hydrolysis. Note that GxxxxGKS/T, WDTAGQE, GNKxD and ETSAK motifs are conserved in the two *N. benthamiana* homologs NbRabG3c-a and NbRabG3c-b. B–D) Immune blots and subcellular localization patterns of GFP fusions of NbRabG3c-a and NbRabG3c-b proteins. 35S::GFP-NbRabG3c-a but not 35S::GFP-NbRabG3c-b showed a similar localization pattern to AtRabG3c at the tonoplast (Ton.), endosomes and weakly at the cytoplasm (Cyt.). E) Perihaustorial accumulation of NbRabG3c-a. 35S::GFP-NbRabG3c-a shows a perihaustorial accumulation and colocalizes with RFP-AVRblb2 at the EHM. Arrowheads point to haustoria. F and G) Tonoplast (Ton.) and endosomal localization of GFP-NbRabG3c-a when expressed from its

native promoter. Endosomes marked by pRabG3c::GFP-NbRabG3c-a overlapped with RFP-ARA7-labeled endosomes. Arrowheads point to the endomembrane compartments where both proteins colocalized. H and I) EHM and endosomal localization of GFP-NbRabG3c-a expressed under the control of its native promoter. pRabG3c::GFP-NbRabG3c-a localized to the tonoplast and the EHM compartments marked by RFP-AVRblb2. pRabG3c::GFP-NbRabG3c-a-labeled endomembrane structures appear around haustoria (h) were not labeled by RFP-AVRblb2. The fluorescence plot (I, right panel) shows relative fluorescence along the dotted line connecting points a and b as shown in the middle panel, highlighting the EHM and perihaustorial tonoplast localization of pRabG3c::GFP-NbRabG3c-a. Magenta marks plastids.

Figure S5: StSERK3 is recruited to EHM compartments. A) Immunoblots of StSERK3-GFP and StSERK3-RFP constructs. B) StSERK3-GFP colocalized with RFP-HaRXL17 at the plasma membrane (PM) and tonoplast (Ton.) inside uninfected cells. Magenta marks plastids. C) StSERK3-GFP colocalized with RFP-AVRblb2 at the PM but not at the tonoplast. D) Perihaustorial distribution of StSERK3 in ~~*Phytophthora infestans* infected~~ host cells. StSERK3-GFP enveloped haustoria marked by RFP-AVRblb2. The fluorescence plot (right panel) shows relative fluorescence along the dotted line connecting points a and b as shown in the middle panel, reflecting localization of StSERK3-GFP at compartments surrounding haustoria. E) In a haustoriated cell where the ~~Ton.~~ did not tightly envelope the haustorium, StSERK3-GFP localized to endosomes across the EHM, which were not labeled by RFP-AVRblb2, although both proteins colocalized at EHM compartments. Teal colored dotted line represents vacuolar membrane ~~Ton.~~ The fluorescence plot (right panel) shows relative fluorescence along the dotted line connecting points a and b as shown in the middle panel, and confirms the colocalization of GFP-StSERK3 and RFP-AVRblb2 at the plasma membrane (PM) and EHM compartments. In addition, StSERK3-GFP signal also peaked at the tonoplast where RFP-AVRblb2 was excluded. F) StSERK3-labeled endosomes across the EHM were marked by AtRabG3c. In haustoriated cells where ~~Ton.~~ is parted away from the EHM StSERK3-RFP-labeled endosomes (pointed by teal arrowheads) that appeared across the EHM were marked by YFP-AtRabG3c. In addition, both YFP-AtRabG3c and StSERK3-RFP showed overlapping signals at EHM compartments in the absence of RFP-AVRblb2. The fluorescence plot (right panel) shows relative fluorescence along the dotted line connecting points a and b as shown in the middle panel, illustrating colocalization of StSERK3-RFP and YFP-AtRabG3c at the Ton. and EHM compartments.

Figure S6: A) FLS2 is excluded from the EHM compartments marked by RFP-AVRblb2, in water-treated control samples. The vacuolar membrane tonoplast, which is shown by a teal-colored representative line, was parted away from the EHM compartments and the plasma membrane labeled by FLS2-GFP and RFP-AVRblb2 (PM). The fluorescence plot (right panel) demonstrates the exclusion of FLS2-GFP from EHM compartments in water-treated control samples. ~~B and C).~~ Activated FLS2-GFP colocalizes with AtRabG3c at endosomes around haustoria. FLS2-GFP was recruited to endosomes around haustoria, which were marked by RFP-AtRabG3c after leaf infiltration with a solution of flgg22 peptide but not with water control ~~(C).~~ Arrowheads point to the perihaustorial endosomes where both proteins colocalize and ~~square~~ with dotted lines illustrates exclusion of FLS2-GFP from haustorial interface. Magenta marks plastids.

Table S1: List of primers used

References

1. Huckelhoven R. Cell wall-associated mechanisms of disease resistance and susceptibility. Annu Rev Phytopathol 2007;45:101–127.
2. Ivanov S, Fedorova E, Bisseling T. Intracellular plant microbe associations: secretory pathways and the formation of perimicrobial compartments. Curr Opin Plant Biol 2010;13:372–377.
3. Valent B, Khang CH. Recent advances in rice blast effector research. Curr Opin Plant Biol 2010;13:434–441.
4. Harrison MJ. Cellular programs for arbuscular mycorrhizal symbiosis. Curr Opin Plant Biol 2012;15:691–698.
5. Frey NFD, Robatzek S. Trafficking vesicles: pro or contra pathogens? Curr Opin Plant Biol 2009;12:437–443.
6. Dodds PN, Rathjen JP. Plant immunity: towards an integrated view of plant-pathogen interactions. Nat Rev Genet 2010;11:539–548.
7. Underwood W, Koh S, Somerville SC. Visualizing cellular dynamics in plant-microbe interactions using fluorescent-tagged proteins. Methods Mol Biol 2011;712:283–291.
8. O'Connell RJ, Panstruga R. Tete a tete inside a plant cell: establishing compatibility between plants and biotrophic fungi and oomycetes. New Phytol 2006;171:699–718.
9. Panstruga R, Dodds PN. Terrific protein traffic: the mystery of effector protein delivery by filamentous plant pathogens. Science 2009;324:748–750.
10. Giraldo MC, Valent B. Filamentous plant pathogen effectors in action. Nat Rev Microbiol 2013;11:800–814.
11. Coffey MD, Wilson UE. Histology and cytology of infection and disease caused by phytophthora. In: Erwin D, Bartnicki-Garcia S, Tsao PH, editors. Phytophthora: Its Biology, Ecology, and Pathology. St Paul, MN: American Phytopathological Society; 1983, pp. 289–301.
12. Micali CO, Neumann U, Grunewald D, Panstruga R, O'Connell R. Biogenesis of a specialized plant-fungal interface during host cell internalization of *Golovinomyces orontii* haustoria. Cell Microbiol 2011;13:210–226.
13. Bozkurt TO, Schornack S, Banfield MJ, Kamoun S. Oomycetes, effectors, and all that jazz. Curr Opin Plant Biol 2012;15:483–492.
14. Mims CW, Richardson EA, Holt BF III, Dangl JL. Ultrastructure of the host-pathogen interface in *Arabidopsis thaliana* leaves infected by the downy mildew *Hyaloperonospora parasitica* (vol 82, pg 1001, 2004). Can J Bot 2004;82:1545.
15. Caillaud MC, Piquerez SJ, Fabro G, Steinbrenner J, Ishaque N, Beynon J, Jones JD. Subcellular localization of the Hpa RxLR effector repertoire identifies a tonoplast-associated protein HaRxL17 that confers enhanced plant susceptibility. Plant J 2012;69:252–265.
16. Fisher MC, Henk DA, Briggs CJ, Brownstein JS, Madoff LC, McCraw SL, Gurr SJ. Emerging fungal threats to animal, plant and ecosystem health. Nature 2012;484:186–194.
17. Yoshida K, Schuenemann VJ, Cano LM, Pais M, Mishra B, Sharma R, Lanz C, Martin FN, Kamoun S, Krause J, Thines M, Weigel D, Burbano HA. The rise and fall of the *Phytophthora infestans* lineage that triggered the Irish potato famine. eLife 2013;2:e00731.

18. Avrova AO, Boevink PC, Young V, Grenville-Briggs LJ, van West P, Birch PR, Whisson SC. A novel *Phytophthora infestans* haustorium-specific membrane protein is required for infection of potato. Cell Microbiol 2008;10:2271–2284.
19. Bozkurt TO, Schornack S, Win J, Shindo T, Ilyas M, Oliva R, Cano LM, Jones AM, Huitema E, van der Hoorn RA, Kamoun S. *Phytophthora infestans* effector AVRblb2 prevents secretion of a plant immune protease at the haustorial interface. Proc Natl Acad Sci U S A 2011;108:20832–20837.
20. Koh S, Andre A, Edwards H, Ehrhardt D, Somerville S. *Arabidopsis thaliana* subcellular responses to compatible *Erysiphe cichoracearum* infections. Plant J 2005;44:516–529.
21. Lu YJ, Schornack S, Spallek T, Geldner N, Chory J, Schellmann S, Schumacher K, Kamoun S, Robatzek S. Patterns of plant subcellular responses to successful oomycete infections reveal differences in host cell reprogramming and endocytic trafficking. Cell Microbiol 2012;14:682–697.
22. Bozkurt TO, Richardson A, Dagdas YF, Mongrand S, Kamoun S, Raffaele S. The plant membrane-associated REM1.3 remorin accumulates in discrete perihaustorial domains and enhances susceptibility to *Phytophthora infestans*. Plant Physiol 2014;165:1005–1018.
23. Pumplin N, Zhang X, Noar RD, Harrison MJ. Polar localization of a symbiosis-specific phosphate transporter is mediated by a transient reorientation of secretion. Proc Natl Acad Sci U S A 2012;109:E665–E672.
24. Nelson JB, O'Hara SP, Small AJ, Tietz PS, Choudhury AK, Pagano RE, Chen XM, LaRusso NF. *Cryptosporidium parvum* infects human cholangiocytes via sphingolipid-enriched membrane microdomains. Cell Microbiol 2006;8:1932–1945.
25. Haldar K, Mohandas N. Erythrocyte remodeling by malaria parasites. Curr Opin Hematol 2007;14:203–209.
26. An Q, Huckelhoven R, Kogel KH, van Bel AJ. Multivesicular bodies participate in a cell wall-associated defence response in barley leaves attacked by the pathogenic powdery mildew fungus. Cell Microbiol 2006;8:1009–1019.
27. Meyer D, Pajonk S, Micali C, O'Connell R, Schulze-Lefert P. Extracellular transport and integration of plant secretory proteins into pathogen-induced cell wall compartments. Plant J 2009;57: 986–999.
28. Takemoto D, Jones DA, Hardham AR. GFP-tagging of cell components reveals the dynamics of subcellular re-organization in response to infection of Arabidopsis by oomycete pathogens. Plant J 2003;33:775–792.
29. Beck M, Zhou J, Faulkner C, MacLean D, Robatzek S. Spatio-temporal cellular dynamics of the Arabidopsis flagellin receptor reveal activation status-dependent endosomal sorting. Plant Cell 2012;24:4205–4219.
30. Beck M, Heard W, Mbengue M, Robatzek S. The INs and OUTs of pattern recognition receptors at the cell surface. Curr Opin Plant Biol 2012;15:367–374.
31. Spallek T, Beck M, Ben Khaled S, Salomon S, Bourdais G, Schellmann S, Robatzek S. ESCRT-I mediates FLS2 endosomal sorting and plant immunity. PLoS Genet 2013;9:e1004035.
32. Choi SW, Tamaki T, Ebine K, Uemura T, Ueda T, Nakano A. RABA members act in distinct steps of subcellular trafficking of the FLAGELLIN SENSING2 receptor. Plant Cell 2013;25:1174–1187.
33. Zipfel C, Robatzek S, Navarro L, Oakeley EJ, Jones JD, Felix G, Boller T. Bacterial disease resistance in Arabidopsis through flagellin perception. Nature 2004;428:764–767.
34. Segonzac C, Zipfel C. Activation of plant pattern-recognition receptors by bacteria. Curr Opin Microbiol 2011;14:54–61.
35. Monaghan J, Zipfel C. Plant pattern recognition receptor complexes at the plasma membrane. Curr Opin Plant Biol 2012;15:349–357.
36. Chinchilla D, Zipfel C, Robatzek S, Kemmerling B, Nurnberger T, Jones JD, Felix G, Boller T. A flagellin-induced complex of the receptor FLS2 and BAK1 initiates plant defence. Nature 2007;448:497–500.
37. Roux M, Schwessinger B, Albrecht C, Chinchilla D, Jones A, Holton N, Malinovsky FG, Tor M, de Vries S, Zipfel C. The Arabidopsis leucine-rich repeat receptor-like kinases BAK1/SERK3 and BKK1/SERK4 are required for innate immunity to hemibiotrophic and biotrophic pathogens. Plant Cell 2011;23:2440–2455.
38. Sun Y, Li L, Macho AP, Han Z, Hu Z, Zipfel C, Zhou JM, Chai J. Structural basis for flg22-induced activation of the Arabidopsis FLS2-BAK1 immune complex. Science 2013;342:624–628.
39. Geldner N, Hyman DL, Wang X, Schumacher K, Chory J. Endosomal signaling of plant steroid receptor kinase BRI1. Genes Dev 2007;21:1598–1602.
40. Chinchilla D, Shan L, He P, de Vries S, Kemmerling B. One for all: the receptor-associated kinase BAK1. Trends Plant Sci 2009;14:535–541.
41. Irani NG, Di Rubbo S, Mylle E, Van den Begin J, Schneider-Pizon J, Hnilikova J, Sisa M, Buyst D, Vilarrasa-Blasi J, Szatmari AM, Van Damme D, Mishev K, Codreanu MC, Kohout L, Strnad M, et al. Fluorescent castasterone reveals BRI1 signaling from the plasma membrane. Nat Chem Biol 2012;8:583–589.
42. Smith JM, Salamango DJ, Leslie ME, Collins CA, Heese A. Sensitivity to Flg22 is modulated by ligand-induced degradation and de novo synthesis of the endogenous flagellin-receptor FLAGELLIN-SENSING2. Plant Physiol 2014;164:440–454.
43. Girard E, Chmiest D, Fournier N, Johannes L, Paul JL, Vedie B, Lamaze C. Rab7 is functionally required for selective cargo sorting at the early endosome. Traffic 2014;15:309–326.
44. Geldner N, Denervaud-Tendon V, Hyman DL, Mayer U, Stierhof YD, Chory J. Rapid, combinatorial analysis of membrane compartments in intact plants with a multicolor marker set. Plant J 2009;59:169–178.
45. Bottanelli F, Gershlick DC, Denecke J. Evidence for sequential action of Rab5 and Rab7 GTPases in prevacuolar organelle partitioning. Traffic 2012;13:338–354.
46. Foresti O, Gershlick DC, Bottanelli F, Hummel E, Hawes C, Denecke J. A recycling-defective vacuolar sorting receptor reveals an intermediate compartment situated between prevacuoles and vacuoles in tobacco. Plant Cell 2010;22:3992–4008.
47. Petre B, Kamoun S. How do filamentous pathogens deliver effector proteins into plant cells? PLoS Biol 2014;12:e1001801.
48. Tyler BM, Tripathy S, Zhang X, Dehal P, Jiang RH, Aerts A, Arredondo FD, Baxter L, Bensasson D, Beynon JL, Chapman J, Damasceno CM, Dorrance AE, Dou D, Dickerman AW, et al. Phytophthora genome

sequences uncover evolutionary origins and mechanisms of pathogenesis. Science 2006;313:1261–1266.
49. Whisson SC, Boevink PC, Moleleki L, Avrova AO, Morales JG, Gilroy EM, Armstrong MR, Grouffaud S, van West P, Chapman S, Hein I, Toth IK, Pritchard L, Birch PR. A translocation signal for delivery of oomycete effector proteins into host plant cells. Nature 2007;450:115–118.
50. Haas BJ, Kamoun S, Zody MC, Jiang RH, Handsaker RE, Cano LM, Grabherr M, Kodira CD, Raffaele S, Torto-Alalibo T, Bozkurt TO, Ah-Fong AM, Alvarado L, Anderson VL, Armstrong MR, et al. Genome sequence and analysis of the Irish potato famine pathogen *Phytophthora infestans*. Nature 2009;461:393–398.
51. Win J, Chaparro-Garcia A, Belhaj K, Saunders DG, Yoshida K, Dong S, Schornack S, Zipfel C, Robatzek S, Hogenhout SA, Kamoun S. Effector biology of plant-associated organisms: concepts and perspectives. Cold Spring Harb Symp Quant Biol 2012;77:235–247.
52. Saunders DG, Breen S, Win J, Schornack S, Hein I, Bozkurt TO, Champouret N, Vleeshouwers VG, Birch PR, Gilroy EM, Kamoun S. Host protein BSL1 associates with *Phytophthora infestans* RXLR effector AVR2 and the *Solanum demissum* immune receptor R2 to mediate disease resistance. Plant Cell 2012;24:3420–3434.
53. Wolfenstetter S, Wirsching P, Dotzauer D, Schneider S, Sauer N. Routes to the tonoplast: the sorting of tonoplast transporters in Arabidopsis mesophyll protoplasts. Plant Cell 2012;24:215–232.
54. Bucherl CA, van Esse GW, Kruis A, Luchtenberg J, Westphal AH, Aker J, van Hoek A, Albrecht C, Borst JW, de Vries SC. Visualization of BRI1 and BAK1(SERK3) membrane receptor heterooligomers during brassinosteroid signaling. Plant Physiol 2013;162:1911–1925.
55. Chaparro-Garcia A, Wilkinson RC, Gimenez-Ibanez S, Findlay K, Coffey MD, Zipfel C, Rathjen JP, Kamoun S, Schornack S. The receptor-like kinase SERK3/BAK1 is required for basal resistance against the late blight pathogen *Phytophthora infestans* in *Nicotiana benthamiana*. PLoS One 2011;6:e16608.
56. Koh S, Somerville S. Show and tell: cell biology of pathogen invasion. Curr Opin Plant Biol 2006;9:406–413.
57. Bednarek P, Kwon C, Schulze-Lefert P. Not a peripheral issue: secretion in plant-microbe interactions. Curr Opin Plant Biol 2010;13:378–387.
58. Faulkner C, Robatzek S. Plants and pathogens: putting infection strategies and defence mechanisms on the map. Curr Opin Plant Biol 2012;15:699–707.
59. Baxt LA, Garza-Mayers AC, Goldberg MB. Bacterial subversion of host innate immune pathways. Science 2013;340:697–701.
60. Randow F, MacMicking JD, James LC. Cellular self-defense: how cell-autonomous immunity protects against pathogens. Science 2013;340:701–706.
61. Goodin MM, Zaitlin D, Naidu RA, Lommel SA. *Nicotiana benthamiana*: its history and future as a model for plant-pathogen interactions. Mol Plant Microbe Interact 2008;21:1015–1026.
62. Woollard AA, Moore I. The functions of Rab GTPases in plant membrane traffic. Curr Opin Plant Biol 2008;11:610–619.
63. Limpens E, Ivanov S, van Esse W, Voets G, Fedorova E, Bisseling T. Medicago N2-fixing symbiosomes acquire the endocytic identity marker Rab7 but delay the acquisition of vacuolar identity. Plant Cell 2009;21:2811–2828.
64. Meresse S, Steele-Mortimer O, Finlay BB, Gorvel JP. The rab7 GTPase controls the maturation of *Salmonella typhimurium*-containing vacuoles in HeLa cells. EMBO J 1999;18:4394–4403.
65. Clemens DL, Lee BY, Horwitz MA. *Mycobacterium tuberculosis* and *Legionella pneumophila* phagosomes exhibit arrested maturation despite acquisition of Rab7. Infect Immun 2000;68:5154–5166.
66. Neunuebel MR, Machner MP. The taming of a Rab GTPase by *Legionella pneumophila*. Small GTPases 2012;3:28–33.
67. Drecktrah D, Knodler LA, Howe D, Steele-Mortimer O. Salmonella trafficking is defined by continuous dynamic interactions with the endolysosomal system. Traffic 2007;8:212–225.
68. Platta HW, Stenmark H. Endocytosis and signaling. Curr Opin Cell Biol 2011;23:393–403.
69. Teis D, Taub N, Kurzbauer R, Hilber D, de Araujo ME, Erlacher M, Offterdinger M, Villunger A, Geley S, Bohn G, Klein C, Hess MW, Huber LA. p14-MP1-MEK1 signaling regulates endosomal traffic and cellular proliferation during tissue homeostasis. J Cell Biol 2006;175:861–868.
70. Hisata S, Sakisaka T, Baba T, Yamada T, Aoki K, Matsuda M, Takai Y. Rap1-PDZ-GEF1 interacts with a neurotrophin receptor at late endosomes, leading to sustained activation of Rap1 and ERK and neurite outgrowth. J Cell Biol 2007;178:843–860.
71. Ewald SE, Lee BL, Lau L, Wickliffe KE, Shi GP, Chapman HA, Barton GM. The ectodomain of Toll-like receptor 9 is cleaved to generate a functional receptor. Nature 2008;456:658–662.
72. Chockalingam A, Brooks JC, Cameron JL, Blum LK, Leifer CA. TLR9 traffics through the Golgi complex to localize to endolysosomes and respond to CpG DNA. Immunol Cell Biol 2009;87:209–217.
73. Nielsen ME, Feechan A, Bohlenius H, Ueda T, Thordal-Christensen H. Arabidopsis ARF-GTP exchange factor, GNOM, mediates transport required for innate immunity and focal accumulation of syntaxin PEN1. Proc Natl Acad Sci U S A 2012;109:11443–11448.
74. Kamoun S, van West P, Vleeshouwers VG, de Groot KE, Govers F. Resistance of *Nicotiana benthamiana* to *Phytophthora infestans* is mediated by the recognition of the elicitor protein INF1. Plant Cell 1998;10:1413–1426.
75. Song J, Win J, Tian M, Schornack S, Kaschani F, Ilyas M, van der Hoorn RA, Kamoun S. Apoplastic effectors secreted by two unrelated eukaryotic plant pathogens target the tomato defense protease Rcr3. Proc Natl Acad Sci U S A 2009;106:1654–1659.
76. Altschul SF, Gish W, Miller W, Myers EW, Lipman DJ. Basic local alignment search tool. J Mol Biol 1990;215:403–410.
77. Larkin MA, Blackshields G, Brown NP, Chenna R, McGettigan PA, McWilliam H, Valentin F, Wallace IM, Wilm A, Lopez R, Thompson JD, Gibson TJ, Higgins DG. Clustal W and Clustal X version 2.0. Bioinformatics (Oxford, England) 2007;23:2947–2948.
78. Nelson BK, Cai X, Nebenfuhr A. A multicolored set of in vivo organelle markers for co-localization studies in Arabidopsis and other plants. Plant J 2007;51:1126–1136.

79. Karimi M, Inze D, Depicker A. GATEWAY vectors for Agrobacterium-mediated plant transformation. Trends Plant Sci 2002;7:193–195.
80. Consortium TPGS. Genome sequence and analysis of the tuber crop potato. Nature 2011;475:189–195.
81. Van der Hoorn RA, Laurent F, Roth R, De Wit PJ. Agroinfiltration is a versatile tool that facilitates comparative analyses of Avr9/Cf-9-induced and Avr4/Cf-4-induced necrosis. Mol Plant Microbe Interact 2000;13:439–446.
82. Oh SK, Young C, Lee M, Oliva R, Bozkurt TO, Cano LM, Win J, Bos JI, Liu HY, van Damme M, Morgan W, Choi D, Van der Vossen EA, Vleeshouwers VG, Kamoun S. In planta expression screens of *Phytophthora infestans* RXLR effectors reveal diverse phenotypes, including activation of the *Solanum bulbocastanum* disease resistance protein Rpi-blb2. Plant Cell 2009;21:2928–2947.
83. R Core Team. R: A Language and Environment for Statistical Computing. Vienna: R Foundation for Statistical ComputingURL http://www.R-project.org/; 2014.